

Limits on the anomalous Wtq couplingsR. Romero Aguilar, Antonio O. Bouzas,^{*} and F. Larios*Departamento de Física Aplicada, CINVESTAV-Mérida, A.P. 73, 97310 Mérida, Yucatán, Mexico*

(Received 21 September 2015; published 1 December 2015)

Within the model-independent framework of $SU(3) \times SU(2) \times U(1)$ gauge-invariant dimension-six operators, we study flavor off-diagonal Wtq couplings ($q = d, s$) and related four-quark contact interactions involving the top. We obtain bounds on those couplings from Tevatron and LHC data for single-top production and branching fractions in top decays, as well as other experimental results on flavor-changing neutral-current processes including $B \rightarrow X_q \gamma$ and $Z \rightarrow b\bar{q}$ decays ($q = d, s$). We also update the bounds on flavor-diagonal Wtb couplings using the most recent measurement of W -helicity fractions in top decays from top-pair production.

DOI: 10.1103/PhysRevD.92.114009

PACS numbers: 14.65.Ha, 12.15.-y

I. INTRODUCTION

Top-quark physics plays an essential role in the research program at the LHC. The top quark and the Higgs boson—being the heaviest known elementary particle and the only known elementary scalar, respectively—may be the best candidates to look for physics beyond the standard model (SM) [1]. We may classify the different studies on the top quark by the type of interactions they consider, either flavor off-diagonal or diagonal. Within the class of flavor-diagonal couplings we can find studies on htt [2], γtt [3,4], Ztt [5], Gtt [6], Wtb [7–10], as well as contact vertices such as $ttqq$, $tbud$, $tbve$ [9,11–13]. For the flavor off-diagonal case, we can find global studies that include top couplings with several or all of the neutral gauge bosons [14–19], as well as more specific works on $htu(c)$ [20], $\gamma tu(c)$ [21], $Ztu(c)$ [22] and $Gtu(c)$ [23] couplings. There are also studies on four-fermion interactions like $tbff'$ and $tdve$ [11,14]. To date, there are no similar studies on experimental limits for the flavor off-diagonal charged-current (CC) Wtq couplings available in the literature.

The main goal of this paper is to fill this gap by obtaining bounds on flavor off-diagonal charged-current couplings of the top quark from available experimental data. We focus on the flavor off-diagonal couplings Wtd and Wts as they arise in the basis of dimension-six $SU(3) \times SU(2) \times U(1)$ gauge-invariant operators involving the top quark. We consider also contact four-quark interactions related to the Wtq couplings through the SM equations of motion. In this work we keep the flavor structure of the theory completely general, by taking the dimension-six couplings as independent parameters. Notice that other theoretical flavor structures have been considered in the literature, such as the minimal flavor violation framework in which the flavor mixing pattern of the SM is extended to the dimension-six Lagrangian [11,24]. In addition to our

analysis of the flavor off-diagonal Wtq vertices we also make an update on the allowed parameter region of the flavor-diagonal Wtb coupling, which has received much attention in the recent literature [7,8,25,26]. We assess the allowed parameter regions for this vertex based on the cross sections for tq and tb production measured at the Tevatron and LHC, and the measurement of W -helicity fractions in top decays from top-pair production most recently reported [27].

A minimal basis of $SU(3) \times SU(2) \times U(1)$ gauge-invariant dimension-six operators involving the top quark has been given in [28,29], and a complete one in [30]. As far as top interactions are concerned those bases are identical, aside from minor differences in the definition of contact four-fermion operators. We use that basis in this paper, as has become standard in the recent literature. We carry out all computations at leading order (LO) in both the SM and dimension-six effective couplings, fully analytically in the case of decays and numerically with MADGRAPH5_AMC@NLO [31] for scattering processes. We adopt the operator normalization established in [17] (and references therein) at next-to-leading-order (NLO), which is applicable also at LO and facilitates the counting of coupling-constant powers, especially for automated computations.

Due to $SU(2) \times U(1)$ gauge invariance and its spontaneous breaking a complete separation of charged and neutral currents in dimension-six operators is not possible. As a consequence, most of the basis operators involve interactions of both types in combinations that may not be optimal to study a given process. For those processes we have to consider suitable linear combinations of basis operators instead of the operators themselves. A similar strategy is used in [14]. For those effective operators containing both CC and neutral-current (NC) terms, we take into account experimental data for processes involving one or both types of vertices. Thus, besides single-top production in hadron collisions (involving only flavor off-diagonal charged-currents in the SM, but also

^{*}Corresponding author.
abouzas@fis.mda.cinvestav.mx

flavor-changing neutral currents (FCNC) in the effective theory) and branching fractions in $t \rightarrow Wq$ decays, we consider also FCNC vertices not involving the top such as γbq in $b \rightarrow d\gamma, s\gamma$ and Zbq in $Z \rightarrow bd, bs$, as well as the FCNC vertices in $t \rightarrow Zu, Zc$ and $pp(gu) \rightarrow t\gamma$ from [14]. In this way, we survey the sensitivity of the different processes to find the ones providing the best bounds for each effective coupling.

The paper is organized as follows. In Sec. II we list the dimension-six gauge-invariant operators relevant to this study. In Sec. III we analyze FCNC decay processes of the top quark, the Z boson and the B meson, as well as flavor off-diagonal top decays $t \rightarrow Wq$, that are used to obtain the limits on the operators. In Sec. IV we discuss the contribution of flavor off-diagonal effective operators to single-top production at the Tevatron and the LHC. In Sec. V we present the results obtained from the processes studied in the previous sections on allowed regions for the Wtd and Wts effective couplings, the flavor-diagonal Wtb couplings, and the four-quark ones. Finally, in Sec. VI we give our conclusions.

II. TOP QUARK DIMENSION-SIX OPERATORS

New physics effects related to the top quark can be described consistently by an effective electroweak Lagrangian that satisfies the full $SU(3)_C \times SU(2)_L \times U(1)_Y$ gauge symmetry of the SM:

$$\mathcal{L} = \mathcal{L}_{\text{SM}} + \frac{1}{\Lambda^2} \sum_k (C_k O_k^{(6)} + \text{H.c.}) + \dots,$$

where the ellipsis stands for operators of dimension higher than six. Λ is the scale of new, or beyond the SM physics. The scale Λ is unknown but we will assume it to be $\Lambda = 1$ TeV as is commonly used in the literature [14,32]. This is a valid assumption given that the physical processes that are being considered are at the significantly lower electroweak scale (m_W, m_t or v). The Wilson coefficients C_k depend on the scale, but in tree level analyses this dependence is not taken into account [33]. As experiments have reached higher precision it has become appropriate to make studies at the next perturbative order, where radiative corrections and renormalization dictate the dependence of C_k on the scale [34]. For instance, in Ref. [17] we can find a study of top quark decay at NLO in QCD where the operator mixing terms that appear at this level are taken into account. In particular, the W -helicity branching fractions of $t \rightarrow bW$ decay at tree level only depend on Wtb operators like O_{uW}^{k3} (defined below) but at NLO they can receive an indirect contribution from the top-gluon operator O_{qG} [17]. Nevertheless, our study is made at tree level for processes at (or below) the top mass scale and we do not take into account the effects of scale running and operator mixing.

Many years ago a long list of gauge invariant dimension-six operators was introduced in Ref. [35]. Eventually, it was found that not all operators there are truly independent

[28,36]. A revised list of independent operators for the top-quark sector appeared first in [28,29], and then a general revised list for all the fields was provided in [30]. Notice that the list of top-gauge boson operators in [28] and in [30] coincide, except for the explicit notation in a few cases (like $O_{\phi\phi}^{ij} \equiv O_{\phi ud}^{ij}$). From now on, we will refer to the effective operators as defined in Ref. [30]. However, we adopt the sign convention in the covariant derivatives as well as the operator normalization defined in [17], where a factor y_i is attached to an operator for each Higgs field it contains, and a factor g (g') for each W (B) field-strength tensor.

As stated previously, we will follow the strategy of Ref. [14], where some of the operators considered there are the same in our work. The original Lagrangian in Eq. (1) is written in terms of gauge eigenstates but we are referring to the physical (mass) eigenstates in our operators. This means that additional Cabibbo-Kobayashi-Maskawa (CKM) suppressed terms appear in the Wtq vertices generated; for example, the original diagonal operator $O_{\phi q}^{(3)33}$ will generate a Wts nondiagonal coupling with a V_{ts} factor. We have taken into account these mixing terms, but we point out that in the end there is only a very small change in the allowed regions of parameters. Notice that there are recent studies on the potential of the LHC to measure CKM matrix elements based on top quark rapidity distribution [37]. Our study is focused on the Wtq vertices that originate in the dimension-six operators.

A. Effective Wtq couplings of the top quark

Flavor indices aside, there are only four operators that give rise to effective Wtq couplings: $O_{\phi q}^{(3)k3}$, $O_{\phi ud}^{3k}$ ($= O_{\phi\phi}^{3k}$ in [28]), O_{uW}^{k3} and O_{dW}^{3k} ($k = 1, 2$). The operator $O_{\phi ud}^{3k}$ involves exclusively a charged-current vertex, but the other three also generate neutral-current couplings:

$$\begin{aligned} O_{\phi q}^{(3)k3} &= \frac{y_t^2}{2\sqrt{2}} g(v+h)^2 (W_\mu^+ \bar{u}_{Lk} \gamma^\mu b'_L + W_\mu^- \bar{d}'_{Lk} \gamma^\mu t_L) \\ &\quad + \frac{y_t^2}{2\sqrt{2}} \frac{g}{c_w} (v+h)^2 Z_\mu (\bar{u}_{Lk} \gamma^\mu t_L - \bar{d}'_{Lk} \gamma^\mu b'_L), \\ O_{uW}^{k3} &= 2y_t g(v+h) (\partial_\mu W_\nu^- + igW_\mu^3 W_\nu^-) \bar{d}'_{Lk} \sigma^{\mu\nu} t_R \\ &\quad + \sqrt{2} y_t g(v+h) (c_w \partial_\mu Z_\nu + s_w \partial_\mu A_\nu + igW_\mu^- W_\nu^+) \\ &\quad \times \bar{u}_{Lk} \sigma^{\mu\nu} t_R, \\ O_{dW}^{3k} &= 2y_t g(v+h) (\partial_\mu W_\nu^+ + igW_\mu^+ W_\nu^3) \bar{t}_L \sigma^{\mu\nu} d_{Rk} \\ &\quad - \sqrt{2} y_t g(v+h) (c_w \partial_\mu Z_\nu + s_w \partial_\mu A_\nu + igW_\mu^- W_\nu^+) \\ &\quad \times \bar{b}'_L \sigma^{\mu\nu} d_{Rk}. \end{aligned} \quad (1)$$

With the aim of isolating NC of the up quarks from those of the down quarks and of separating the Z field from the photon field A , we consider appropriate linear combinations of $O_{\phi q}^{(3)k3}$, O_{uW}^{k3} and O_{dW}^{3k} with the purely NC operators $O_{\phi q}^{(1)k3}$, O_{uB}^{k3} and O_{dB}^{3k} . This strategy was also

used in [14], where the FCNC interactions of the top quark were analyzed. We therefore base our analysis on the following operators, written here in terms of the physical vector boson fields:

$$\begin{aligned}
O_{\varphi q}^{(+)k3} &= O_{\varphi q}^{(1)k3} + O_{\varphi q}^{(3)k3} \\
&= \frac{y_t^2}{2\sqrt{2}} g(v+h)^2 (W_\mu^+ \bar{u}_{Lk} \gamma^\mu b'_L + W_\mu^- \bar{d}'_{Lk} \gamma^\mu t_L) \\
&\quad - \frac{y_t^2}{2} \frac{g}{c_W} (v+h)^2 Z_\mu \bar{d}'_{Lk} \gamma^\mu b'_L, \\
O_{\varphi q}^{(-)k3} &= O_{\varphi q}^{(1)k3} - O_{\varphi q}^{(3)k3} \\
&= -\frac{y_t^2}{2\sqrt{2}} g(v+h)^2 (W_\mu^+ \bar{u}_{Lk} \gamma^\mu b'_L + W_\mu^- \bar{d}'_{Lk} \gamma^\mu t_L) \\
&\quad - \frac{y_t^2}{4} \frac{g}{c_W} (v+h)^2 Z_\mu \bar{u}_{Lk} \gamma^\mu t_L, \\
O_{\varphi ud}^{3k} &= \frac{y_t^2}{2\sqrt{2}} g(v+h)^2 W_\mu^+ \bar{t}_R \gamma^\mu d_{Rk}, \\
O_{uZ}^{k3} &= O_{uW}^{k3} - O_{uB}^{k3} \\
&= 2y_t g(v+h) (\partial_\mu W_\nu^- + igW_\mu^3 W_\nu^-) \bar{d}'_{Lk} \sigma^{\mu\nu} t_R \\
&\quad + \sqrt{2} y_t g(v+h) \left(\frac{1}{c_W} \partial_\mu Z_\nu + igW_\mu^- W_\nu^+ \right) \bar{u}_{Lk} \sigma^{\mu\nu} t_R, \\
O_{dZ}^{3k} &= O_{dW}^{3k} + O_{dB}^{3k} \\
&= 2y_t g(v+h) (\partial_\mu W_\nu^+ + igW_\mu^+ W_\nu^3) \bar{t}_L \sigma^{\mu\nu} d_{Rk} \\
&\quad + \sqrt{2} y_t g(v+h) \left(-\frac{1}{c_W} \partial_\mu Z_\nu + igW_\mu^+ W_\nu^- \right) \\
&\quad \times \bar{b}'_L \sigma^{\mu\nu} d_{Rk}, \\
O_{uA}^{k3} &= s_W^2 O_{uW}^{k3} + c_W^2 O_{uB}^{k3} = 2y_t g s_W^2 (v+h) \\
&\quad \times (\partial_\mu W_\nu^- + igW_\mu^3 W_\nu^-) \bar{d}'_{Lk} \sigma^{\mu\nu} t_R \\
&\quad + \sqrt{2} y_t g s_W^2 (v+h) \left(\frac{1}{s_W} \partial_\mu A_\nu + igW_\mu^- W_\nu^+ \right) \\
&\quad \times \bar{u}_{Lk} \sigma^{\mu\nu} t_R, \\
O_{dA}^{3k} &= s_W^2 O_{dW}^{3k} - c_W^2 O_{dB}^{3k} \\
&= 2y_t g s_W^2 (v+h) (\partial_\mu W_\nu^+ + igW_\mu^+ W_\nu^3) \bar{t}_L \sigma^{\mu\nu} d_{Rk} \\
&\quad + \sqrt{2} y_t g s_W^2 (v+h) \left(-\frac{1}{s_W} \partial_\mu A_\nu + igW_\mu^+ W_\nu^- \right) \\
&\quad \times \bar{b}'_L \sigma^{\mu\nu} d_{Rk}. \tag{2}
\end{aligned}$$

Standard notation is used in this equation, with I, J, K SU(2) gauge indices, τ^I the Pauli matrices, and φ the SM Higgs doublet with $\tilde{\varphi} = i\tau^2 \varphi^*$. The covariant derivative is defined as $D_\mu \varphi = \partial_\mu \varphi - ig/2 \tau^I W_\mu^I \varphi - ig'/2 B_\mu \varphi$ [14,17]. The primed quark fields d', s', b' , are gauge eigenfields related to mass eigenfields through the CKM matrix. In Eq. (2), operators with $k = 1, 2$ yield flavor off-diagonal effective Wtq couplings, while those with $k = 3$ correspond to

flavor-diagonal CC interactions. (The latter have been considered in [7,8,25,26].) From the point of view of Wtq interactions, the four operators $O_{\varphi q}^{(-)k3}, O_{\varphi ud}^{3k}, O_{uZ}^{k3}, O_{dZ}^{3k}$ in (2) are completely equivalent to the original ones $O_{\varphi q}^{(3)k3}, O_{\varphi ud}^{3k}, O_{uW}^{k3}, O_{dW}^{3k}$ given in (1) as listed in [28,30]. Notice that the operators O_{uA}^{k3} and O_{dA}^{3k} contain the same CC vertices as O_{uZ}^{k3} and O_{dZ}^{3k} . For the case of O_{dA}^{3k} , the radiative decay $b \rightarrow q\gamma$ happens to be very sensitive to this vertex as it contributes at tree level, and we will be able to show limits of order 10^{-5} which are much stronger than any of the other bounds. We will then, neglect the potential effects of the CC vertex of O_{dA}^{3k} to single top production. In the case of O_{uA}^{k3} , as mentioned in [14] the CMS measurement of the parton level $gq \rightarrow t\gamma$ production process yields strong constraints as well, and we will also be able to neglect its potential effects. This will also allow us to avoid t -channel photon-exchange diagrams that would lead to divergent total cross sections.

The relations between the coefficients of the original operators $O_{\varphi q}^{(1)k3}, O_{\varphi q}^{(3)k3}, O_{uW}^{k3}, O_{dW}^{3k}, O_{uB}^{k3}, O_{dB}^{3k}$, and the new ones are given by:

$$\begin{aligned}
\begin{pmatrix} C_{\varphi q}^{(+)k3} \\ C_{\varphi q}^{(-)k3} \end{pmatrix} &= \frac{1}{2} \begin{pmatrix} 1 & 1 \\ 1 & -1 \end{pmatrix} \begin{pmatrix} C_{\varphi q}^{(1)k3} \\ C_{\varphi q}^{(3)k3} \end{pmatrix}, \\
\begin{pmatrix} C_{uA}^{k3} \\ C_{uZ}^{k3} \end{pmatrix} &= \begin{pmatrix} 1 & 1 \\ -s_W^2 & c_W^2 \end{pmatrix} \begin{pmatrix} C_{uB}^{k3} \\ C_{uW}^{k3} \end{pmatrix}, \\
\begin{pmatrix} C_{dA}^{3k} \\ C_{dZ}^{3k} \end{pmatrix} &= \begin{pmatrix} -1 & 1 \\ s_W^2 & c_W^2 \end{pmatrix} \begin{pmatrix} C_{dB}^{3k} \\ C_{dW}^{3k} \end{pmatrix}.
\end{aligned}$$

For concreteness, in the rest of this paper we set $\Lambda \equiv 1$ TeV, and write the dimensionful parameters in the operators in units of TeV, namely, $v = 0.246$, $m_t = 0.1725$ and $m_W = 0.0804$. We will show the limits on these coefficients below, but in addition we will translate them to the limits on the form factors $V_{L(R)}$ and $g_{L(R)}$ that are commonly used in the literature for the diagonal Wtb vertex [7,8,38,39]. We will extend the definition to the flavor off-diagonal Wtq couplings: $V_{L(R)}^q$ and $g_{L(R)}^q$. The relation between the form factors and the operator coefficients is given by:

$$\begin{aligned}
V_L^q &= V_{tq} + \frac{y_t^2}{2} \frac{v^2}{\Lambda^2} (C_{\varphi q}^{(+)k3} - C_{\varphi q}^{(-)k3}) \\
&= V_{tq} + (C_{\varphi q}^{(+)k3} - C_{\varphi q}^{(-)k3})/33.606, \\
V_R^q &= \frac{y_t^2}{2} \frac{v^2}{\Lambda^2} C_{\varphi ud}^{3k} = C_{\varphi ud}^{3k}/33.606, \\
-g_R^q &= \sqrt{2} g y_t \frac{v^2}{\Lambda^2} (C_{uZ}^{k3} + s_W^2 C_{uA}^{k3}) \\
&= (C_{uZ}^{k3} + s_W^2 C_{uA}^{k3})/18.156, \\
-g_L^q &= \sqrt{2} g y_t \frac{v^2}{\Lambda^2} (C_{dZ}^{3k} + s_W^2 C_{dA}^{3k}) \\
&= (C_{dZ}^{3k} + s_W^2 C_{dA}^{3k})/18.156, \tag{3}
\end{aligned}$$

where $q = d(s)$ corresponds to $k = 1(2)$. The form factors $V_{L(R)}^q$ and $g_{L(R)}^q$ for $q = b$ are equivalent to $f_1^{L(R)}$ and $-f_2^{L(R)}$ in [25,40]. Notice that the contributions by C_{uA}^{3k} to g_R^q are suppressed by the s_W^2 factor, which is a desirable feature as we are neglecting its effect on single-top production.

B. Four-quark operators

The choice of independent Wtq operators in [28,30] could have included another operator: $O_{qW}^{ij} = \bar{q}_{Li}\gamma^\mu\tau^a D^\nu q_{Lj} W_{\mu\nu}^a$ that is associated with an off-shell W -propagator contribution to single top quark production [9,29]. However, since O_{qW}^{ij} is related through the equations of motion to four-fermion operators, we choose to include the latter in our basis of independent operators. Bases for the $SU(2) \times U(1)$ -gauge invariant dimension-six four-quark operators have been given in [29,30]. The four-quark operators related to O_{qW}^{ij} involve left quarks only. In the notation of [30] the four-left-quark basis operators are given by:

$$\begin{aligned} O_{qq}^{(1)ijkl} &= (\bar{q}_{Li}\gamma_\mu q_{Lj})(\bar{q}_{Lk}\gamma^\mu q_{Ll}), \\ O_{qq}^{(3)ijkl} &= (\bar{q}_{Li}\gamma_\mu\tau^l q_{Lj})(\bar{q}_{Lk}\gamma^\mu\tau^l q_{Ll}). \end{aligned} \quad (4)$$

Other chiral structures can also contribute to single top production, some of them have been considered in [11]. The operators (4) involving the first and third families that we consider in this paper are

$$\begin{aligned} O_{qq}^{(1)1113} &= (\bar{u}_L\gamma_\mu u_L + \bar{d}'_L\gamma_\mu d'_L)(\bar{u}_L\gamma^\mu t_L + \bar{d}'_L\gamma^\mu b'_L), \\ O_{qq}^{(3)1113} &= 2(\bar{u}_L\gamma_\mu d'_L)(\bar{d}'_L\gamma^\mu t_L) + 2(\bar{d}'_L\gamma_\mu u_L)(\bar{u}_L\gamma^\mu b'_L) \\ &\quad + (\bar{u}_L\gamma_\mu u_L - \bar{d}'_L\gamma_\mu d'_L)(\bar{u}_L\gamma^\mu t_L - \bar{d}'_L\gamma^\mu b'_L), \\ O_{qq}^{(1)3113} &= (\bar{t}_L\gamma_\mu u_L + \bar{b}'_L\gamma_\mu d'_L)(\bar{u}_L\gamma^\mu t_L + \bar{d}'_L\gamma^\mu b'_L), \\ O_{qq}^{(3)3113} &= 2(\bar{t}_L\gamma_\mu d'_L)(\bar{d}'_L\gamma^\mu t_L) + 2(\bar{b}'_L\gamma_\mu u_L)(\bar{u}_L\gamma^\mu b'_L) \\ &\quad + (\bar{t}_L\gamma_\mu u_L - \bar{b}'_L\gamma_\mu d'_L)(\bar{u}_L\gamma^\mu t_L - \bar{d}'_L\gamma^\mu b'_L), \\ O_{qq}^{(1)1133} &= (\bar{u}_L\gamma_\mu u_L + \bar{d}'_L\gamma_\mu d'_L)(\bar{t}_L\gamma^\mu t_L + \bar{b}'_L\gamma^\mu b'_L), \\ O_{qq}^{(3)1133} &= 2(\bar{d}'_L\gamma_\mu u_L)(\bar{t}_L\gamma^\mu b'_L) + 2(\bar{u}_L\gamma_\mu d'_L)(\bar{b}'_L\gamma^\mu t_L) \\ &\quad + (\bar{u}_L\gamma_\mu u_L - \bar{d}'_L\gamma_\mu d'_L)(\bar{t}_L\gamma^\mu t_L - \bar{b}'_L\gamma^\mu b'_L), \\ O_{qq}^{(1)3313} &= (\bar{t}_L\gamma_\mu t_L + \bar{b}'_L\gamma_\mu b'_L)(\bar{u}_L\gamma^\mu t_L + \bar{d}'_L\gamma^\mu b'_L), \\ O_{qq}^{(3)3313} &= 2(\bar{t}_L\gamma_\mu b'_L)(\bar{d}'_L\gamma^\mu t_L) + 2(\bar{b}'_L\gamma_\mu t_L)(\bar{u}_L\gamma^\mu b'_L) \\ &\quad + (\bar{t}_L\gamma_\mu t_L - \bar{b}'_L\gamma_\mu b'_L)(\bar{u}_L\gamma^\mu t_L - \bar{d}'_L\gamma^\mu b'_L), \end{aligned} \quad (5)$$

with $O_{qq}^{(1,3)3113}$ and $O_{qq}^{(1,3)1133}$ Hermitian. All of the operators (5) are relevant to single-top production, except for $O_{qq}^{(1)3113} + O_{qq}^{(3)3113}$ and $O_{qq}^{(1)1133}$ which contain only terms

with an even number of top fields and can be bounded by their contribution to top-pair production. The operators

$$\begin{aligned} O_{qq}^{(1)1313} &= (\bar{u}_L\gamma_\mu t_L + \bar{d}'_L\gamma_\mu b'_L)(\bar{u}_L\gamma^\mu t_L + \bar{d}'_L\gamma^\mu b'_L), \\ O_{qq}^{(3)1313} &= 4(\bar{u}_L\gamma_\mu b'_L)(\bar{d}'_L\gamma^\mu t_L) \\ &\quad + (\bar{u}_L\gamma_\mu t_L - \bar{d}'_L\gamma_\mu b'_L)(\bar{u}_L\gamma^\mu t_L - \bar{d}'_L\gamma^\mu b'_L), \end{aligned} \quad (6)$$

comprise single-top and two-top vertices. The ATLAS Collaboration [41] has obtained tight limits on the operators (6), through the term $(\bar{u}_L\gamma_\mu t_L)(\bar{u}_L\gamma^\mu t_L)$, from its measurement of the same-sign top production cross section (see Sec. V D below).

We see from Eq. (23) of [28] that $O_{qq}^{(1)1133}$, $O_{qq}^{(3)3113}$, $O_{qq}^{(1)3113}$ enter the decomposition into basis operators of the flavor-diagonal operators O_{qW}^{11} and O_{qW}^{33} , and both $O_{qq}^{(3)1113}$ and $O_{qq}^{(3)3313}$ that of the flavor off-diagonal operator O_{qW}^{13} . If we denote by O_{qq} , $O_{qq'}$ the four left-quark operators in the basis of [29], they are related to those in (4) by $O_{qq}^{\text{ijkl}} = 1/2 O_{qq}^{(1)ijkl}$ and $O_{qq'}^{\text{ijkl}} = 1/4(O_{qq}^{(3)ilkj} + O_{qq}^{(1)ilkj})$ [29]. We point out also that the four-quark operator considered in [7] is $\hat{O}_{qq'}^{(3)} = O_{qq'}^{(3)1133}$.

III. LIMITS FROM DECAY PROCESSES

In this section we discuss the limits on effective couplings that come from several FCNC processes as well as those from observables associated to $t \rightarrow Wq$ decays. A global analysis of FCNC top-quark interactions is given in [14], including NLO QCD corrections [17,18], in which many processes with direct contributions from effective top vertices are surveyed to find those yielding the best bounds on effective couplings. Here, we restrict ourselves to a simplified analysis involving only the two processes that play the most important role in setting bounds for the operators $O_{qq}^{(-)k3}$, O_{uZ}^{k3} and O_{uA}^{k3} : the on-shell $t \rightarrow jZ$ decay and the single top $pp \rightarrow t\gamma$, $\bar{t}\gamma$ production. With these two experimental inputs we will be able to obtain constraints similar to those in [14]. In addition, we consider also two FCNC processes that are not associated to the top but to the bottom quark: $B \rightarrow X_q\gamma$ and $Z \rightarrow b\bar{q}$. These will provide bounds on the operators O_{dA}^{k3} , O_{dZ}^{k3} and $O_{\phi q}^{(+)k3}$.

A. Limits from FCNC processes

Let us briefly describe how we can obtain bounds for the NC part of the operators. We will start with the ones that do not involve the top quark but the bottom quark.

The main contribution to the radiative decay $B \rightarrow X_q\gamma$ comes from the operator $O_7 = \frac{e}{16\pi^2} m_b \bar{q}_L \sigma^{\mu\nu} b_R F_{\mu\nu}$ with

$q = d, s$, involving the right-handed b quark and the left-handed light quark q . However, there is also a (smaller) contribution from the right-handed q operator O_7^R . We observe that the operator O_{dA}^{3k} directly (at tree level) contributes to O_7^R at the electroweak scale, with:

$$-\frac{4G_F}{\sqrt{2}}V_{tb}V_{tq}^*\frac{e}{16\pi^2}m_b C_7^R = C_{dA}^{3k}y_t\frac{g_S W}{\sqrt{2}}\frac{v}{\Lambda^2} \quad (7)$$

In Ref. [42] (Eq. 42) we can find a specific expression that singles out the contribution from C_7^R :

$$\text{Br}(B \rightarrow X_q \gamma) = \text{Br}^{\text{SM}}(B \rightarrow X_q \gamma) + 1.22 \times 10^{-2} |V_{tq}|^2 \left| \frac{C_7^R}{C_7^{\text{SM}}} \right|^2 \quad (8)$$

where $C_7^{\text{SM}}(\mu = m_t) = -0.189$, $V_{td} = 0.0088$, $V_{ts} = 0.0405$, and the SM values for the branching fractions are given as [42]:

$$10^4 \text{Br}^{\text{SM}}(B \rightarrow X_s \gamma) = 3.61 \pm 0.4, \\ 10^5 \text{Br}^{\text{SM}}(B \rightarrow X_d \gamma) = 1.38 \pm 0.22.$$

We can use the experimental results [43]:

$$10^4 \text{Br}^{\text{exp}}(B \rightarrow X_s \gamma) = 3.43 \pm 0.21 \pm 0.07, \\ 10^5 \text{Br}^{\text{exp}}(B \rightarrow X_d \gamma) = 0.92 \pm 0.30,$$

to set the limits $|C_7^{Rd}| < 0.32$ and $|C_7^{Rs}| < 0.36$ at 95% C.L. When we translate these limits for the C_{dA} coefficients we get an extra suppression from the CKM matrix elements:

$$C_{dA}^{31} < 0.96 \times 10^{-5}, \quad C_{dA}^{32} < 5.4 \times 10^{-5}. \quad (9)$$

These are the strongest limits we have obtained for any of the effective operators. FCNC processes will also provide the strongest constraints to all but the $O_{\phi ud}$ operator as we shall see next.

Operators $O_{\phi q}^{(+k3)}$ and O_{dZ} with an effective Zbq coupling contribute directly to $Z \rightarrow b\bar{q}$ decays ($q = d, s$). We can use the (90% C.L.) LEP upper limit [44]

$$R_{bl} = \frac{\sum_{q=d,s} \sigma(e^+e^- \rightarrow b\bar{q}, \bar{b}q)}{\sigma(e^+e^- \rightarrow \text{hadrons})} \leq 2.6 \times 10^{-3} \quad (10)$$

to set bounds on these coefficients. Numerically, we can write

$$\frac{\Gamma(Z \rightarrow b\bar{q}, \bar{b}q)}{\Gamma(Z \rightarrow \text{hadrons})} = (2.63|C_{\phi q}^{(+13)}|^2 + 2.86|C_{dZ}^{31}|^2) \times 10^{-3} + (13 \rightarrow 23), \quad (11)$$

and obtain the following bounds

$$1.0(|C_{\phi q}^{(+13)}|^2 + |C_{\phi q}^{(+23)}|^2) + 1.1(|C_{dZ}^{31}|^2 + |C_{dZ}^{32}|^2) \leq 1.0. \quad (12)$$

There are also (indirect) stringent bounds coming from the $\text{Br}(B_d \rightarrow \mu^+ \mu^-)$ and $\text{Br}(B_s \rightarrow \mu^+ \mu^-)$ measurements [45]: $|C_{\phi q}^{(+13)}| < 0.005$ and $|C_{\phi q}^{(+23)}| < 0.015$.

The remaining operators that can be constrained with top-quark FCNC processes are $O_{\phi q}^{(-k3)}$, O_{uZ}^{k3} and O_{uA}^{k3} . In Ref. [14] there is a thorough analysis based on the $t \rightarrow jZ$ decay including off-shell contributions. Let us simplify our discussion and consider the on-shell $\text{Br}(t \rightarrow jZ)$ only:

$$\text{Br}(t \rightarrow jZ) = 3.34 \times 10^{-4} \Sigma_{k=1,2} \times \left(\left| \frac{C_{\phi q}^{(-k3)}}{2x} - 2x C_{uZ}^{k3} \right|^2 + 2 \left| \frac{C_{\phi q}^{(-k3)}}{2} - 2 C_{uZ}^{k3} \right|^2 \right)$$

with $x = m_Z/m_t$ ($2x = 1.05$). The (95% C.L.) experimental upper bound is $\text{Br}(t \rightarrow jZ) < 5.0 \times 10^{-4}$ [46], therefore

$$\Sigma_{k=1,2} \left(\left| \frac{C_{\phi q}^{(-k3)}}{2x} - 2x C_{uZ}^{k3} \right|^2 + 2 \left| \frac{C_{\phi q}^{(-k3)}}{2} - 2 C_{uZ}^{k3} \right|^2 \right) < 1.5. \quad (13)$$

For the other operator O_{uA}^{k3} the CMS collaboration has measured the process $\sigma(pp \rightarrow t\gamma, \bar{t}\gamma)$ that provides the most stringent limit to date [14]:

$$0.460|C_{uA}^{13}|^2 + 0.037|C_{uA}^{23}|^2 < 0.067. \quad (14)$$

Equations (9), (12), (13) and (14) will be used to define the allowed parameter regions for the Wtq couplings. They are based on the NC part of the dimension six operators. Below, we will describe the processes and experimental values where the CC part plays the leading role.

B. Limits from CC processes

We turn next to the charge-current decays $t \rightarrow Wq$, $q = d, s, b$. Specifically, in this section we discuss the total width, the branching ratios and W -helicity fractions in top decay. From a theoretical standpoint, it has been reported that the $t \rightarrow Wq$ decay could get a 50% enhancement in the context of the MSSM [47], which underscores the importance of top decay measurements like the ratio of $\text{Br}(t \rightarrow Wb)$ to $\text{Br}(t \rightarrow Wq)$ [48].

In terms of form factors, the $t \rightarrow qW$ width for each helicity of the W boson, including terms proportional to m_q , is given by [25,38,40,49]:

$$\begin{aligned}
\Gamma_0 &= A[|a_t V_L^q - g_R^q|^2 + |a_t V_R^q - g_L^q|^2 + a_q G_0^q], \\
\Gamma_+ &= A[2|V_R^q - a_t g_L^q|^2 + a_q G_+^q], \\
\Gamma_- &= A[2|V_L^q - a_t g_R^q|^2 + a_q G_-^q], \\
A &= \frac{g^2 m_t}{64\pi} \left(1 - \frac{m_W^2}{m_t^2}\right),
\end{aligned} \tag{15a}$$

with

$$\begin{aligned}
G_0^q &= [(a_t^2 + 1)(M_L^q + M_R^q) - 2a_t M_{LR}^q]/(a_t^2 - 1), \\
G_{+(-)}^q &= M_{L(R)}^q - M_{R(L)}^q + G_0^q, \\
M_{LR}^q &= 2\text{Re}\{V_L^q V_R^{q*} + g_L^q g_R^{q*}\}, \\
M_{L(R)}^q &= 2\text{Re}\{V_{L(R)}^q g_{L(R)}^{q*}\},
\end{aligned} \tag{15b}$$

where $a_t = m_t/m_W$ and so is $a_q = m_q/m_W$ for any down type quark. NLO QCD corrections (for $m_b = 0$) to these W -helicity widths can be found in [50]. We can use the expressions (15) to obtain the ratio $\text{Br}(t \rightarrow Wb)/\sum \text{Br}(t \rightarrow Wq)$, the total decay width, and the W -helicity branching fractions.

The recent experimental measurement [48] of the ratio:

$$\mathcal{R} \equiv \frac{\text{Br}(t \rightarrow Wb)}{\sum \text{Br}(t \rightarrow Wq)} = 1.014 \pm 0.003(\text{stat}) \pm 0.032(\text{syst}),$$

is given by CMS also as a 95% C.L. lower bound $\mathcal{R} > 0.955$ once the condition $\mathcal{R} \leq 1$ has been imposed [48] (see also [51,52] for previous Tevatron results). We use this experimental lower bound on \mathcal{R} to obtain the following bounds at 95% C.L.:

$$\begin{aligned}
&\begin{cases} |C_{\varphi q}^{(\pm)k3}|, |C_{\varphi ud}^{3k}| < 7.29 \\ |C_{uZ}^{k3}|, |C_{dZ}^{3k}| < 3.16 \end{cases}, \quad (k = 1, 2), \\
\text{or} &\begin{cases} V_L^q, V_R^q < 0.22 \\ f_R^q, f_L^q < 0.17 \end{cases}, \quad (q = d, s),
\end{aligned} \tag{16}$$

given here for convenience for both effective couplings and form factors.

Equation (15) also yields the W -helicity fractions in $t \rightarrow bW$ decays:

$$F_0 = \Gamma_0/\Gamma, \quad F_L = \Gamma_-/\Gamma. \tag{17}$$

$F_{0,L}$ are the most sensitive observables to the flavor-diagonal couplings $C_{\varphi ud}^{33}$, C_{uZ}^{33} , C_{dZ}^{33} , as has long been known and duly exploited in the recent phenomenological literature [7,8]. In this paper we take into account the recent measurement of W -helicity fractions in top decays from $t\bar{t}$ production at 8 TeV, with 20 fb⁻¹ of data collected at the LHC [27], which constitutes an improvement from previous measurements [39]. We obtain bounds for each

effective coupling at 95% C.L. from the measured W -helicity fractions by means of a likelihood analysis for the two correlated observables $F_{0,L}$, as detailed in Eqs. (18)–(20) of [7]. From the CMS results [27],

$$\begin{aligned}
F_0 &= 0.653 \pm 0.016(\text{stat}) \pm 0.024(\text{syst}), \\
F_L &= 0.329 \pm 0.009(\text{stat}) \pm 0.025(\text{syst}),
\end{aligned} \tag{18}$$

we get the single-coupling bounds:

$$\begin{aligned}
&\begin{cases} |C_{\varphi ud}^{33}| < 5.38, & |C_{dZ}^{33}| < 1.27 \\ -0.73 < C_{uZr}^{33} < 1.63, & |C_{uZi}^{33}| < 4.36 \end{cases}, \\
\text{or} &\begin{cases} |V_R| < 0.16, & |g_L| < 0.07 \\ -0.09 < g_{Rr} < 0.04, & |g_{Ri}| < 0.24. \end{cases}
\end{aligned} \tag{19}$$

The partial widths (15a) do not depend on the left-handed vector couplings $C_{\varphi q}^{(\pm)33}$ (or, equivalently, V_L) if the other effective couplings vanish, so no single-coupling bounds are obtained. From the indirect measurement of the total top width [48] we obtain:

$$\begin{aligned}
&-3.02 < C_{\varphi qr}^{(\pm)33} < 3.7, \quad |\delta C_{\varphi qi}^{(\pm)33}| < 16.13, \\
\text{or} &-0.09 < \delta V_{Lr} < 0.11, \quad |\delta V_{Li}| < 0.48.
\end{aligned}$$

As discussed below, stronger bounds on $C_{\varphi q}^{(\pm)33}$ result from single-top production cross section.

IV. SINGLE-TOP QUARK PRODUCTION

The effective operators (2) contribute to the single top production processes $pp \rightarrow tq$ (with q a quark lighter than b) and $p\bar{p} \rightarrow t\bar{b}$, and to the associated production process $p\bar{p} \rightarrow tW$, through both their CC and NC vertices. Furthermore, the four-quark operators (5) contribute to the first two types of single-top production. In this section we discuss single-top production assuming for simplicity a diagonal CKM mixing matrix, to keep the diagrams down to a manageable number. Alternatively, the diagrams in Figs. 1–6 can be considered as given in the weak-interaction quark basis.

The Feynman diagrams for the process $pp \rightarrow tq$ are shown in Figs. 1 and 2. In the SM, ignoring CKM mixing, only the $t\bar{b}W$ CC vertex can lead to single-top production in pp collisions, resulting in the four Feynman diagrams shown in Fig. 1(a). Each one of the operators $O_{\varphi q}^{(\pm)33}$, $O_{\varphi ud}^{33}$, O_{dZ}^{33} or O_{uZ}^{33} contains a flavor-diagonal CC vertex, leading to four SM-like diagrams with an effective $t\bar{b}W$ vertex, Fig. 1(b). Flavor off-diagonal charged-current effective vertices from the operators $O_{\varphi q}^{(\pm)j3}$, $O_{\varphi ud}^{3j}$, O_{dZ}^{3j} or O_{uZ}^{j3} lead to four t -channel and two s -channel diagrams for each operator type and each value of $j = 1, 2$, Fig. 1(c). The operators $O_{\varphi q}^{(\pm)j3}$ ($j = 1, 2$) contain a flavor off-diagonal

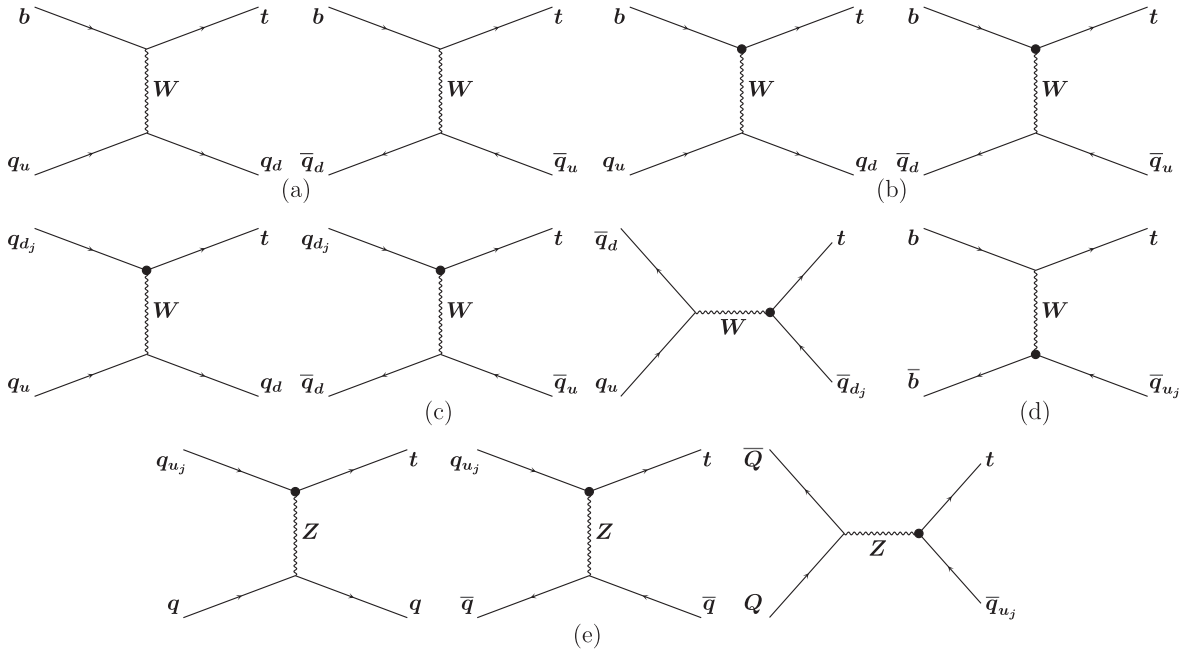


FIG. 1. Feynman diagrams for the process $pp \rightarrow tq$. (a) SM diagrams, neglecting CKM mixing. (b) One flavor-diagonal CC effective vertex proportional to $C_{\phi q}^{(\pm)33}$, $C_{\phi ud}^{33}$, C_{dZ}^{33} or C_{uZ}^{33} ($q_u, q_d = u, d$ or c, s). (c) One flavor off-diagonal charged-current effective vertex proportional to $C_{\phi q}^{(\pm)j3}$, $C_{\phi ud}^{3j}$, C_{dZ}^{3j} or C_{uZ}^{j3} ($j = 1, 2$). (d) One flavor off-diagonal charged-current effective vertex proportional to $C_{\phi q}^{(\pm)j3}$ ($j = 1, 2$). (e) One flavor-changing NC effective vertex proportional to $C_{\phi q}^{(-)j3}$ or C_{uZ}^{j3} ($j = 1, 2$; $q = u, d, c, s$; $Q = q, b$).

charged-current effective vertex for the b quark, giving rise to the diagram in Fig. 1(d). The flavor-changing NC effective vertices contained in $O_{\phi q}^{(-)j3}$, O_{uZ}^{j3} induce nine t/u -channel and five s -channel diagrams mediated by a Z boson for each operator type and each value of $j = 1, 2$, Fig. 1(e).

We point out here that the operator O_{uW}^{j3} ($j = 1, 2$) would lead to an additional set of diagrams analogous to those in Fig. 1(d), but mediated by a photon instead of a Z boson. The γ -mediated t -channel diagrams lead to a Coulomb divergence in the full phase-space cross section, which is the reason why we must consider the operators O_{uZ}^{j3} instead

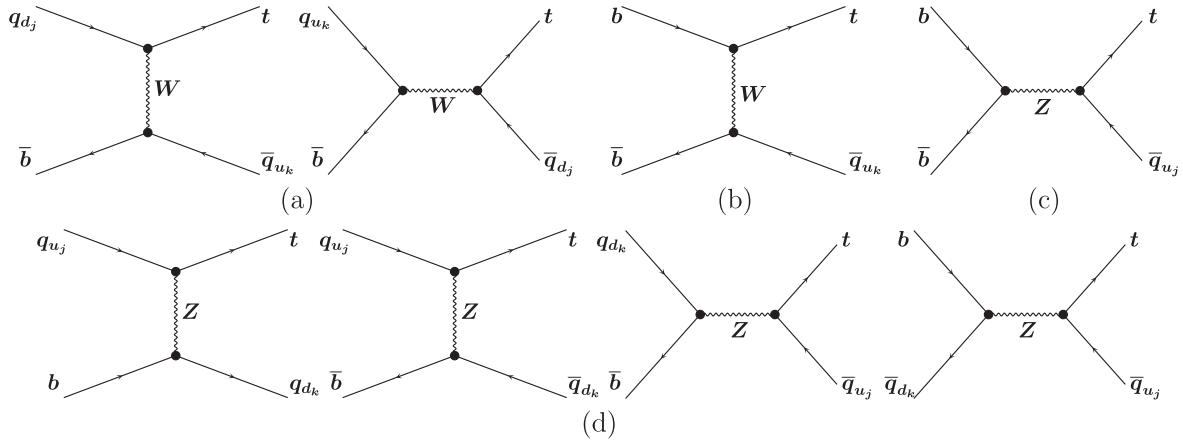


FIG. 2. Feynman diagrams for the process $pp \rightarrow tq$ with two effective vertices. (a) Two flavor off-diagonal charged-current vertices, one proportional to $C_{\phi q}^{(\pm)k3}$ and one proportional to $C_{\phi q}^{(\pm)j3}$, $C_{\phi ud}^{3j}$, C_{dZ}^{3j} or C_{uZ}^{j3} , $k, j = 1, 2$. (b) Two CC vertices, a flavor off-diagonal one proportional to $C_{\phi q}^{(\pm)k3}$, $k = 1, 2$, and a flavor-diagonal one proportional to $C_{\phi q}^{(\pm)33}$, $C_{\phi ud}^{33}$, C_{dZ}^{33} or C_{uZ}^{33} . (c) Two NC vertices, a flavor-diagonal one proportional to $C_{\phi q}^{(+33)}$ or C_{dZ}^{33} , and a flavor-changing one proportional to $C_{\phi q}^{(-)j3}$ or C_{uZ}^{j3} , $j = 1, 2$. (d) Two flavor-changing NC vertices, one proportional to $C_{\phi q}^{(+k3)}$ or C_{dZ}^{3k} and one proportional to $C_{\phi q}^{(-)j3}$ or C_{uZ}^{j3} , $k, j = 1, 2$.

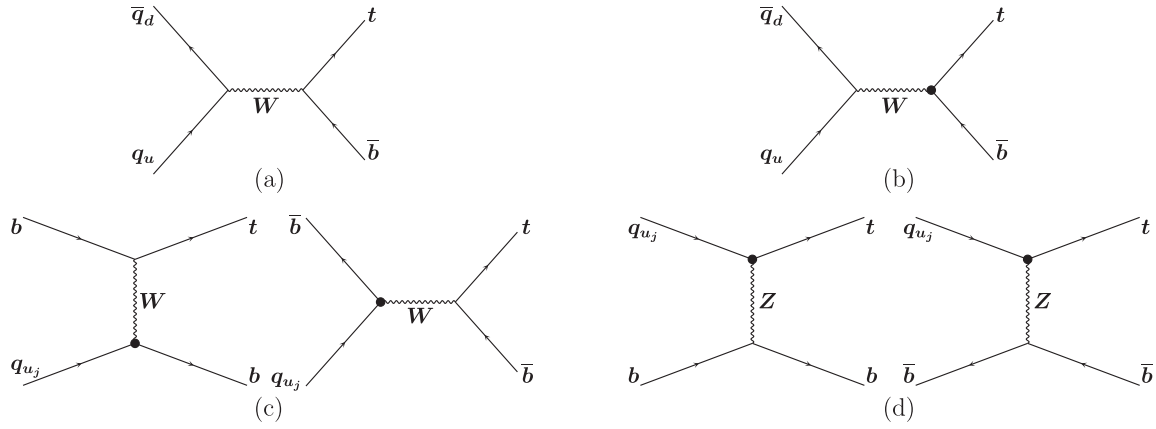


FIG. 3. Feynman diagrams for the process $pp \rightarrow tb, t\bar{b}$ with less than two effective vertices. (a) SM diagram. (b) One flavor-diagonal CC effective vertex proportional to $C_{\varphi q}^{(\pm)33}$, $C_{\varphi ud}^{33}$, C_{dZ}^{33} or C_{uZ}^{33} . (c) One flavor off-diagonal charged-current vertex effective proportional to $C_{\varphi q}^{(\pm)j3}$. (d) One FCNC effective vertex proportional to $C_{\varphi q}^{(-)j3}$ or $C_{uZ}^{(+)j3}$. ($j = 1, 2$.)

of O_{uW}^{j3} . Notice that the extrapolation of detector-level experimental data to a parton-level cross section for $pp \rightarrow tq$ in full phase space, as given in [53–55], involves the explicit assumption of validity of the SM in which flavor-changing photon vertices are absent.

The operators $O_{\varphi q}^{(\pm)k3}$ ($k = 1, 2, 3$) contain flavor diagonal and off-diagonal CC vertices involving a b quark that induce diagrams with two effective CC vertices, as shown in Figs. 2(a) and 2(b). Furthermore, $O_{\varphi q}^{(+)n3}$ and O_{dW}^{3n} ($n = 1, 2, 3$) contain flavor diagonal and off-diagonal NC vertices involving a b quark which, combined with the flavor-changing NC vertices involving t in $O_{\varphi q}^{(-)j3}$ and O_{uZ}^{j3} ($j = 1, 2$) lead to the Z -mediated diagrams with two effective vertices shown in Figs. 2(c) and 2(d). We take

into account in our analysis these diagrams with two effective vertices, to check that their contributions are indeed small within the allowed regions in coupling space, as discussed below.

The process $p\bar{p} \rightarrow tb$ also involves contributions from both flavor off-diagonal and diagonal tWq vertices. The associated Feynman diagrams involving one and two effective vertices are displayed in Figs. 3 and 4, for which a description completely analogous to the one given for the two previous figures applies. As for the associated tW production, it turns out not to play a relevant role in our results so we do not dwell further on it here for brevity.

In Fig. 5 we show the Feynman diagrams for $pp \rightarrow tq$ arising from the four-quark vertices from the operators (5). As seen in the figure, in principle all three types of

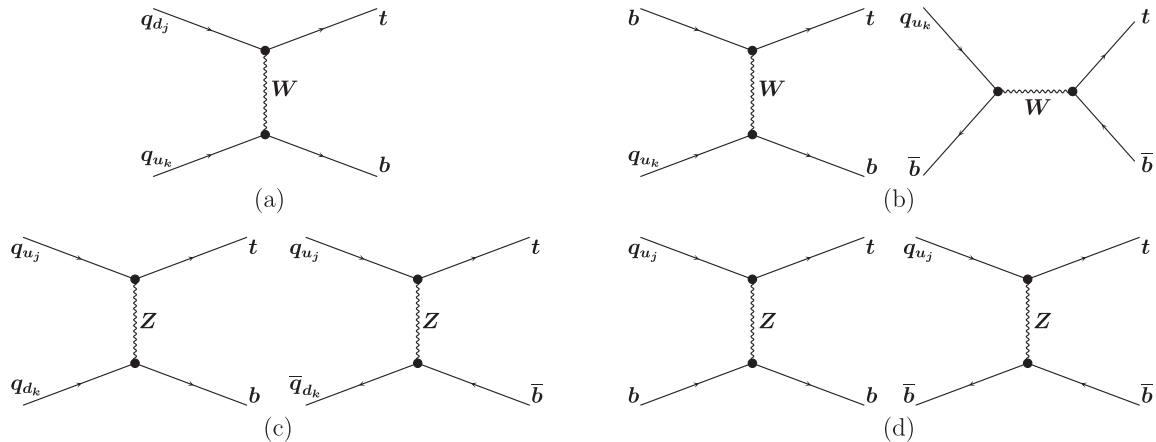


FIG. 4. Feynman diagrams for the process $pp \rightarrow tb, t\bar{b}$ with two effective vertices. (a) Two flavor off-diagonal charged-current vertices, one proportional to $C_{\varphi q}^{(\pm)k3}$ and one to $C_{\varphi q}^{(\pm)j3}$, $C_{\varphi ud}^{3j}$, C_{dZ}^{3j} or C_{uZ}^{j3} . (b) Two CC vertices, a flavor off-diagonal one proportional to $C_{\varphi q}^{(\pm)k3}$ and a flavor-diagonal one proportional to $C_{\varphi q}^{(\pm)33}$, $C_{\varphi ud}^{33}$, C_{dZ}^{33} or C_{uZ}^{33} . (c) Two flavor-changing NC vertices, one proportional to $C_{\varphi q}^{(+)k3}$ or C_{dZ}^{3k} and one to $C_{\varphi q}^{(-)k3}$ or C_{uZ}^{j3} . (d) Two NC vertices, a flavor-diagonal one proportional to $C_{\varphi q}^{(+)33}$ or C_{dZ}^{33} and a flavor-changing one proportional to $C_{\varphi q}^{(-)j3}$ or C_{uZ}^{j3} . In all cases $k, j = 1, 2$.

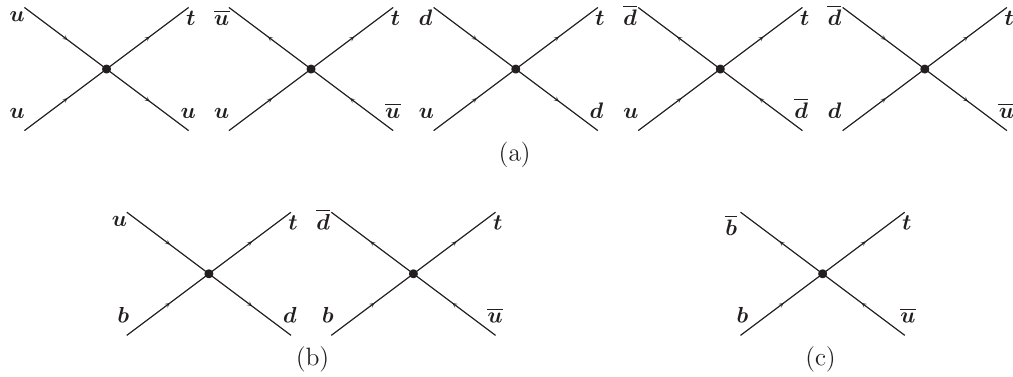


FIG. 5. Feynman diagrams for the process $pp \rightarrow tq$ with one contact-interaction four-quark vertex (a) proportional to $C_{qq}^{(1)1113}$ or $C_{qq}^{(3)1113}$, (b) proportional to $C_{qq}^{(1)3113}$ or $C_{qq}^{(3)1133}$, (c) proportional to $C_{qq}^{(1)3313}$ or $C_{qq}^{(3)3313}$.

operators (involving three, two and one light quark, respectively) in (5) contribute to this process. It is apparent from Fig. 5(c), however, that the sensitivity of tq production to operators with a single light quark must be negligibly small due to the small parton distribution function (PDF) of the b quark. The contribution of the four-quark operators with two and one light quarks to $p\bar{p} \rightarrow tb, t\bar{b}$ production is shown in Fig. 6. It is in connection with these diagrams that tb production plays its most important role in this paper, since it furnishes the only available limits on the four-quark couplings (5) with a single light quark and the tightest ones on those with two light quarks. In this section we have restricted our discussion of four-quark operators to those involving only first- and third-generation quarks for brevity. However, the extension of Eq. (5) and diagrams 5, 6 to include second-generation quarks is straightforward. In Sec. V below we discuss, besides the operators (5), also those four-quark couplings involving second-generation quarks to which single-top production possesses significant sensitivity.

In our computations of single-top production cross sections we always take into account the decay vertex $t \rightarrow bW$, not shown in Figs. 1–4 for simplicity, which can proceed through the SM vertex or flavor-diagonal effective ones. This leads to the cross section $\sigma(pp \rightarrow tq \rightarrow bWq) = \sigma(pp \rightarrow tq)\text{Br}(t \rightarrow bW)$, with $\text{Br}(t \rightarrow bW)$ the branching fraction for this decay mode. If we restrict ourselves to flavor-diagonal effective operators the decay vertex is irrelevant, since $\text{Br}(t \rightarrow bW)$ cannot depend on

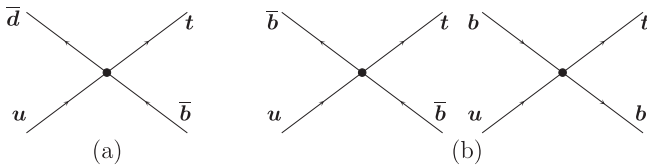


FIG. 6. Feynman diagrams for the process $pp \rightarrow tb, t\bar{b}$ with one contact-interaction four-quark vertex (a) proportional to $C_{qq}^{(1)3113}$ or $C_{qq}^{(3)1133}$, (b) proportional to $C_{qq}^{(1)3313}$ or $C_{qq}^{(3)3313}$.

flavor-diagonal couplings and therefore it cancels in the ratio $\sigma_{\text{eff}}/\sigma_{\text{SM}}$ of the effective and SM cross sections. When, as in this study, flavor off-diagonal vertices are considered, the branching fraction cannot be ignored since it does depend on those couplings. We find that the dependence of $\text{Br}(t \rightarrow bW)$ on the off-diagonal effective couplings tends to relax the bounds on those couplings relative to the ones that would be obtained from the pure production cross section, without including top decay, by up to 15% for operators involving first-generation quarks.

The effective cross section for single-top production can be expressed perturbatively as a power series in the effective couplings. As seen from Figs. 1–4, the cross section for production and decay receives contributions from the effective vertices up to the sixth power in the dim-6 effective couplings. Higher powers arise from the additional dependence of the top propagator on effective couplings. We have explicitly verified in all the cases discussed below that, for values of the effective couplings within their allowed regions, the effect of terms with powers higher than quadratic is negligibly small.

Due to the GIM mechanism for FCNC and to the smallness of CKM third-generation mixing in flavor off-diagonal charged-currents, flavor off-diagonal processes involving the top quark are strongly suppressed at tree level (and beyond) in the SM. For that reason, terms linear in flavor off-diagonal dim-6 effective couplings in the cross section [$\mathcal{O}(1/\Lambda^2)$] are negligibly small since they arise from the interference of amplitudes involving a dim-6 effective vertex with the SM amplitude. By the same token, the contributions to the cross section at order $1/\Lambda^4$ of flavor off-diagonal dim-8 operators are also suppressed. At that order, however, there can be contributions from dim-8 flavor-diagonal operators interfering with the SM which, although expected to be small, are currently unknown and constitute an inherent uncertainty of the EFT analysis.

On the other hand, that uncertainty does not affect the flavor-diagonal couplings $C_{\phi q}^{(\pm)33}$ and C_{uZ}^{33} , which contribute to the single-top production cross section dominantly

through linear terms at order $1/\Lambda^2$ from interference with the SM model. The other two flavor-diagonal couplings, C_{qud}^{33} and C_{dW}^{33} , have their linear interference terms suppressed by m_b and, therefore, significantly smaller.

A. Statistical analysis

Let the experimental and theoretical SM cross sections for single top production in pp or $p\bar{p}$ collisions be

$$\begin{aligned} \sigma_{\text{exp}} \begin{matrix} +\Delta\sigma_{\text{exp}}^{\uparrow} \\ -\Delta\sigma_{\text{exp}}^{\downarrow} \end{matrix} &= \sigma_{\text{exp}} \times \begin{pmatrix} +\epsilon_{\text{exp}}^{\uparrow} \\ -\epsilon_{\text{exp}}^{\downarrow} \end{pmatrix}, \\ \sigma_{\text{thr}} \begin{matrix} +\Delta\sigma_{\text{thr}}^{\uparrow} \\ -\Delta\sigma_{\text{thr}}^{\downarrow} \end{matrix} &= \sigma_{\text{thr}} \times \begin{pmatrix} +\epsilon_{\text{thr}}^{\uparrow} \\ -\epsilon_{\text{thr}}^{\downarrow} \end{pmatrix}, \end{aligned} \quad (20)$$

where we have allowed for asymmetrical uncertainties. The theoretical cross section σ_{thr} is assumed to be computed in the SM, possibly at NNLO + NNLL (e.g., [56–58]). We denote by $\tilde{\sigma}(\lambda)$ the cross section in the effective theory, computed at LO in the effective couplings λ and at the same order as σ_{thr} in the SM couplings, so that $\tilde{\sigma}(0) = \sigma_{\text{thr}}$. Furthermore, we denote by $\sigma(\lambda)$ the cross section in the effective theory computed at LO in both the effective couplings and the SM, and $K(\lambda) = \tilde{\sigma}(\lambda)/\sigma(\lambda)$, so that $K(0)$ is the K -factor in the SM. We base our analysis on the inequalities

$$\tilde{\sigma}(\lambda) - \tilde{\sigma}(0) \leq \sigma_{\text{exp}} - \sigma_{\text{thr}} \begin{matrix} +\sqrt{\sigma_{\text{exp}}^2 \epsilon_{\text{exp}}^{\uparrow 2} + \sigma_{\text{thr}}^2 \epsilon_{\text{thr}}^{\downarrow 2}} \\ -\sqrt{\sigma_{\text{exp}}^2 \epsilon_{\text{exp}}^{\downarrow 2} + \sigma_{\text{thr}}^2 \epsilon_{\text{thr}}^{\uparrow 2}} \end{matrix}. \quad (21)$$

Dividing both sides by σ_{thr} we get,

$$\frac{K(\lambda) \sigma(\lambda)}{K(0) \sigma(0)} \leq R_{\text{exp}} \begin{pmatrix} +\sqrt{\epsilon_{\text{exp}}^{\uparrow 2} + \epsilon_{\text{thr}}^{\downarrow 2}/R_{\text{exp}}^2} \\ -\sqrt{\epsilon_{\text{exp}}^{\downarrow 2} + \epsilon_{\text{thr}}^{\uparrow 2}/R_{\text{exp}}^2} \end{pmatrix}, \quad (22)$$

with $R_{\text{exp}} = \sigma_{\text{exp}}/\sigma_{\text{thr}}$. In (22) the factor $K(\lambda)/K(0) = 1 + \mathcal{O}(\alpha_s \lambda)$, so at LO in the SM we set it to 1. Thus, finally, at LO in both the effective and the SM couplings, we get

$$\frac{\sigma(\lambda)}{\sigma(0)} \leq R_{\text{exp}} \begin{pmatrix} +\sqrt{\epsilon_{\text{exp}}^{\uparrow 2} + \epsilon_{\text{thr}}^{\downarrow 2}/R_{\text{exp}}^2} \\ -\sqrt{\epsilon_{\text{exp}}^{\downarrow 2} + \epsilon_{\text{thr}}^{\uparrow 2}/R_{\text{exp}}^2} \end{pmatrix}. \quad (23)$$

On the right-hand side we identify the ratio R_{exp} of cross sections for single-top production and decay $t \rightarrow bW$ with the ratio of production cross sections, from which it differs by multiplication of both numerator and denominator by $\text{Br}(t \rightarrow bW) = |V_{tb}|^2 \pm \mathcal{O}(10^{-4})$. On the left-hand side of (23) the LO cross section $\sigma(\lambda)$ enters only through the ratio $R(\lambda) = \sigma(\lambda)/\sigma(0)$, which does not depend on the tree-level cross section normalization. Furthermore, for small values of λ , the relative scale and PDF uncertainties are much smaller for $R(\lambda)$ than for the cross sections themselves.

We point out, parenthetically, that (21) is different from the similarly-looking equation

$$\sigma(\lambda) - \sigma(0) \leq \sigma_{\text{exp}} - \sigma_{\text{thr}} \begin{matrix} +\sqrt{\sigma_{\text{exp}}^2 \epsilon_{\text{exp}}^{\uparrow 2} + \sigma_{\text{thr}}^2 \epsilon_{\text{thr}}^{\downarrow 2}} \\ -\sqrt{\sigma_{\text{exp}}^2 \epsilon_{\text{exp}}^{\downarrow 2} + \sigma_{\text{thr}}^2 \epsilon_{\text{thr}}^{\uparrow 2}} \end{matrix}. \quad (24)$$

This inequality does depend on the tree-level cross section normalization. Equation (24) can be rewritten as

$$\begin{aligned} \frac{\sigma(\lambda)}{\sigma(0)} &\leq K(0) R_{\text{exp}} \begin{pmatrix} +\sqrt{\epsilon_{\text{exp}}^{\uparrow 2} + \epsilon_{\text{thr}}^{\downarrow 2}/R_{\text{exp}}^2} \\ -\sqrt{\epsilon_{\text{exp}}^{\downarrow 2} + \epsilon_{\text{thr}}^{\uparrow 2}/R_{\text{exp}}^2} \end{pmatrix} \\ &+ 1 - K(0), \end{aligned} \quad (25)$$

which is different from (23), in particular, because it depends explicitly on $K(0)$, and therefore also on the normalization of the tree-level cross section. In the case of the single-top production cross sections for combined $tq + \bar{t}q$ production measured at the LHC, from the SM results of [56] and our tree-level results we get $K(0) = 1.07$. As a result, the bounds on effective couplings determined by (23) are only slightly tighter than those obtained from (25). On the other hand, for tb production at the Tevatron, from the SM result of [58] we get $K(0) = 1.67$, which leads to significantly more restrictive bounds obtained from (23) than from (25).

V. RESULTS

In this section we present the results obtained from the processes considered in Secs. III and IV, as single-coupling limits and as two-coupling allowed regions for Wtq , Wtb and four-quark effective interactions. Our results are based on the cross sections for tq production measured by CMS:

$$\begin{aligned} \sigma(pp \rightarrow tq + \bar{t}q) &= (67.2 \pm 6.1) \text{ pb}, & 7 \text{ TeV}, 2.73 \text{ fb}^{-1} & \text{ [53]}, \\ \left\{ \begin{aligned} \sigma(pp \rightarrow tq + \bar{t}q) &= (83.6 \pm 7.75) \text{ pb} \\ \sigma(pp \rightarrow tq) &= (53.8 \pm 4.65) \text{ pb}, \\ \sigma(pp \rightarrow \bar{t}q) &= (27.6 \pm 3.92) \text{ pb} \end{aligned} \right. & 8 \text{ TeV}, 19.7 \text{ fb}^{-1} & \text{ [54]}, \end{aligned} \quad (26)$$

together with the NNLO SM predictions from [56,59]

$$\begin{cases} \sigma(pp \rightarrow tq + \bar{t}q) = \begin{pmatrix} 64.6 & +2.1 & +1.5 \\ & -0.6 & -1.7 \end{pmatrix} \text{ pb, } 7 \text{ TeV,} \\ \sigma(pp \rightarrow tq + \bar{t}q) = \begin{pmatrix} 87.2 & +2.8 & +2.0 \\ & -1.0 & -2.2 \end{pmatrix} \text{ pb} \\ \sigma(pp \rightarrow tq) = \begin{pmatrix} 56.4 \pm & +2.1 \\ & -0.3 \end{pmatrix} \pm 1.1 \text{ pb} \quad , \quad 8 \text{ TeV.} \\ \sigma(pp \rightarrow \bar{t}q) = \begin{pmatrix} 30.7 \pm 0.7 & +0.9 \\ & -1.1 \end{pmatrix} \text{ pb.} \end{cases} \quad (27)$$

Further results on the tq production cross section at 7 TeV at the LHC, and on differential cross sections, have been given by ATLAS [55]. We comment on those data below in Sec. V C. The cross section for tb production has been measured by CDF and D0:

$$\sigma(p\bar{p} \rightarrow t\bar{b} + \bar{t}b) = \begin{pmatrix} 1.29 & +0.26 \\ & -0.24 \end{pmatrix} \text{ pb,} \\ 1.96 \text{ TeV, } 19.4 \text{ fb}^{-1} [60], \quad (28)$$

and computed at NNLO in the SM in [58]:

$$\sigma(pp \rightarrow t\bar{b} + \bar{t}b) = (1.05 \pm 0.06) \text{ pb, } 1.96 \text{ TeV.} \quad (29)$$

Notice that tb production has also been observed at the LHC [61,62]. We have also taken into account the associated tW production cross section measured by CMS [63,64], for which an approximate NNLO SM result is given in [65]. We include as well in our results the measurements of W -helicity fractions in top decays, top decay width and ratio of branching fractions $\text{Br}(t \rightarrow Wb) / \sum \text{Br}(t \rightarrow Wq)$ discussed in Sec. III B, as well as the various decay processes in Sec. III A.

Some four-quark operators receive bounds from the $t\bar{t}$ production cross section (see Sec. V D below). In those cases we use the experimental measurements:

$$\begin{aligned} \sigma(pp \rightarrow t\bar{t}) &= (239 \pm 12.7) \text{ pb, } 8 \text{ TeV, } 5.3 \text{ fb}^{-1} [66], \\ \sigma(pp \rightarrow t\bar{t}) &= (158.1 \pm 11) \text{ pb, } 7 \text{ TeV, } 2.3 \text{ fb}^{-1} [67], \\ \sigma(p\bar{p} \rightarrow t\bar{t}) &= (7.6 \pm 0.41) \text{ pb, } 1.96 \text{ TeV, } 8.8 \text{ fb}^{-1} [68], \end{aligned} \quad (30)$$

together with the NNLO SM results:

$$\begin{aligned} \sigma(pp \rightarrow t\bar{t}) &= \begin{pmatrix} 252.9 & +13.3 \\ & -14.5 \end{pmatrix} \text{ pb, } 8 \text{ TeV, } [69, 70], \\ \sigma(pp \rightarrow t\bar{t}) &= \begin{pmatrix} 163 & +11.4 \\ & -10.3 \end{pmatrix} \text{ pb, } 7 \text{ TeV, } [57], \\ \sigma(p\bar{p} \rightarrow t\bar{t}) &= \begin{pmatrix} 7.35 & +0.28 \\ & -0.33 \end{pmatrix} \text{ pb, } 1.96 \text{ TeV, } [69, 70], \end{aligned} \quad (31)$$

as quoted by the experimental collaborations. NNLO SM results for $t\bar{t}$ production at 7 TeV have also been given in [71,72], which are consistent with the values quoted above.

We compute the tree-level cross sections for single-top production and decay with the matrix-element Monte Carlo program MADGRAPH5_AMC@NLO version 2.2.3 [31,73]. The effective operators were implemented in MADGRAPH5 by means of the UFO [74] interface of the program FEYNRULES version 2.0.33 [75]. In all cases we set $m_t = 172.5 \text{ GeV}$, $m_b = 4.7 \text{ GeV}$, $m_Z = 91.1735 \text{ GeV}$, $m_W = 80.401 \text{ GeV}$, $m_h = 125 \text{ GeV}$, $\alpha(m_Z) = 1/132.507$, $G_F = 1.1664 \times 10^{-5} \text{ GeV}^{-2}$, $\alpha_S(m_Z) = 0.118$, and the Higgs vacuum expectation value $v = 246.22 \text{ GeV}$. We set the renormalization and factorization scales fixed at $\mu_R = m_t = \mu_F$ and use the parton-distribution functions CTEQ6-L1 as implemented in MADGRAPH5. The new physics scale Λ is set to 1 TeV. Furthermore, we take into account full CKM mixing in our computations, though its effects on our results are very limited. As expected, third-generation mixing is negligible and could be safely ignored. For values of the effective couplings within the allowed regions obtained here, Cabibbo mixing becomes relevant only for certain four-quark operators, as discussed in more detail below.

A. Limits on flavor off-diagonal couplings

In Table I we gather 95% C.L. limits on flavor off-diagonal Wtq effective couplings taken to be nonzero one at a time. All operators in (2) involve both W and Z/A bosons, except for O_{qud}^{3k} . Thus, in the table we show limits originating from processes involving vertices Vtq with V a charged or neutral vector boson, and with q a first-generation quark (upper two rows) or second-generation one (lower two rows). On the first row we give the best bounds on those couplings involving flavor off-diagonal charged-current vertices Wtd , obtained from CMS data for single t production at 8 TeV [54]. The cross section for combined $t + \bar{t}$ production at the same energy leads to somewhat weaker bounds, as seen in the figures below. The tightest limits for effective couplings associated to the flavor off-diagonal charged-current vertices Wts stem from the ratio of top branching fractions $\text{Br}(t \rightarrow Wb) / \sum_q \text{Br}(t \rightarrow Wq)$ [48], and are shown on the third row of the table. We remark that direct bounds on C_{qud}^{3k} , $k = 1, 2$, have

TABLE I. Limits on the seven operators that are relevant for the study on Wtq couplings. A comparison is made between limits coming from processes involving flavor off-diagonal charged-current interactions (first and third rows) and purely FCNC processes (second and fourth rows).

		$ C_{qud}^{3k} $	$ C_{\varphi q}^{(-)k3} $	$ C_{uZ}^{k3} $	$ C_{uA}^{k3} $	$ C_{\varphi q}^{(+k3)} $	$ C_{dZ}^{3k} $	$ C_{dA}^{3k} $
$k = 1$	Wtd	5.30	2.68	1.37	–	4.95	1.96	–
	$Z(A)tu$	–	1.09	0.42	0.38	1.00	0.95	0.96×10^{-5}
$k = 2$	Wts	7.29	7.29	3.16	–	7.29	3.16	–
	$Z(A)tc$	–	1.08	0.42	1.35	1.00	0.95	5.4×10^{-5}
		no NC		up-quark FCNC			down-quark FCNC	

not been given in the previous literature. However, an indirect limit $|C_{\varphi ud}^{31}| < 5 \times 10^{-3}$ is given in [76] based on the contribution of $O_{\varphi ud}^{31}$ to $b \rightarrow d\gamma$.

On the second and fourth rows of Table I we display the bounds on those same couplings obtained from FCNC processes. For the bounds on operators $O_{\varphi q}^{(+k3)}$ and O_{dZ}^{3k} we have used the decay $Z \rightarrow b\bar{d}(\bar{s})$ in Eq. (12). Operators O_{dA}^{3k} contribute directly to $\text{Br}(B \rightarrow X_q\gamma)$ and for them we obtain the strongest bounds in this study as seen in Eq. (9). For the bounds on operators $O_{\varphi q}^{(-)k3}$ and O_{uZ}^{3k} we have used the decay $t \rightarrow Zu(c)$ (with on-shell Z) in Eq. (13) [14]. Finally, the best bounds on O_{uA}^{3k} come from the FCNC single top production process $\sigma(pp \rightarrow t\gamma, \bar{t}\gamma)$ [14].

Besides the single-coupling bounds in Table I we consider also several allowed two-parameter regions. In Fig. 7 we display allowed regions for pairs of effective couplings having nonvanishing interference (C_{qud}^{3k}/C_{dZ}^{3k} and $C_{qud}^{(-)k3}/C_{uZ}^{k3}$, $k = 1, 2$) and for vector couplings ($C_{qud}^{3k}/C_{\varphi q}^{(-)k3}$). Those regions are obtained at 95% C.L., as described in Sec. IV A, from the production cross section for $tq + \bar{t}q$, with q lighter than b , in pp collisions at 7 TeV [53] (red hatched area in the figure), from the production cross section for $tq + \bar{t}q$ at 8 TeV [54] (black dashed line), from the intersection of the regions allowed by the production cross sections for tq , $\bar{t}q$ and $tq + \bar{t}q$ at 8 TeV [54] (green hatched area), and from the ratio of branching fractions $\text{Br}(t \rightarrow Wb)/\sum_q \text{Br}(t \rightarrow Wq)$ in t decay [48] (orange hatched area). Also shown in the figure, for comparison, are the bounds on C_{dZ}^{3k} and $C_{qud}^{(-)k3}$ from FCNC processes as given in Table I [black dotted lines in Figs. 7(a)–7(d)], and the allowed region for $C_{\varphi q}^{(-)k3}/C_{uZ}^{k3}$ from the branching fraction $\text{Br}(t \rightarrow jZ)$ as given by (13) [black dotted lines in Figs. 7(e)–7(f)].

The cross section for tb production has been measured at the Tevatron [60,77] and at the LHC [61,62]. The production process (see Figs. 3, 4) does not depend on C_{qud}^{3k} , C_{dZ}^{3k} and has a modest sensitivity to $C_{qud}^{(\pm)k3}$, C_{uZ}^{k3} . In fact, for tb production followed by $t \rightarrow Wb$ decay, most of the sensitivity to the effective couplings originates in the dependence on them of the branching fraction $\text{Br}(t \rightarrow Wb)$, which is

already explicitly taken into account in Fig. 7. For this reason we do not include tb production in this figure. We have also taken into account tW associated production, whose cross section has been measured at the LHC at 7 and 8 TeV [63,64]. Due to the somewhat large current experimental uncertainties in those measurements (30% at 7 and 23% at 8 TeV), the allowed regions resulting from this process are significantly looser than those shown in the figure, so we omit them for the sake of simplicity.

In Fig. 8 we show the allowed regions on the plane of the flavor off-diagonal charged-current right-handed vector couplings C_{qud}^{3k} , $k = 1, 2$, and the flavor diagonal left- and right-handed vector couplings $C_{\varphi ud}^{33}$ and $C_{\varphi q}^{(-)33}$. The allowed regions are determined by the same experimental data as used in the previous figure. In Figs. 8(a), 8(b) we include for reference the bounds on C_{qud}^{33} set by the experimental determination of W helicity fractions in t decays [27,39] (black dotted lines in the figure), as discussed in more detail below. In the case of the flavor-diagonal coupling $C_{\varphi q}^{(-)33}$, the best bounds result from a combination of single-top production cross sections at 7 and 8 TeV [53,54] as seen in the figure. We remark that for the processes used in the figure the operators $O_{\varphi q}^{(+33)}$ and $-O_{\varphi q}^{(-)33}$ are equivalent, so the coupling $C_{\varphi q}^{(+33)}$ can be used equally well instead of $-C_{\varphi q}^{(-)33}$ to label the horizontal axes in Figs. 8(c) and 8(d).

B. Limits on the Wtb couplings

In Fig. 9 we show allowed regions for all possible pairs of Wtb effective couplings. As noticed above in connection with Fig. 8, in this context the coupling $C_{\varphi q}^{(+33)}$ is equivalent to $-C_{\varphi q}^{(-)33}$. We obtain the bounds in this figure from the same set of cross sections for single-top production together with a light jet at the LHC [53,54] as in Fig. 7. Also shown in this figure (as light-gray areas) are the allowed regions resulting from the cross section for $p\bar{p} \rightarrow t\bar{b} + \bar{t}b$ measured at the Tevatron [60] (see also [77] for related Tevatron results, and [61,62] for measurements at the LHC). As seen in Fig. 9, the most restrictive limits on the couplings C_{qud}^{33} , C_{uZ}^{33} , C_{dZ}^{33} are imposed by the combination of W -helicity fractions and decay width

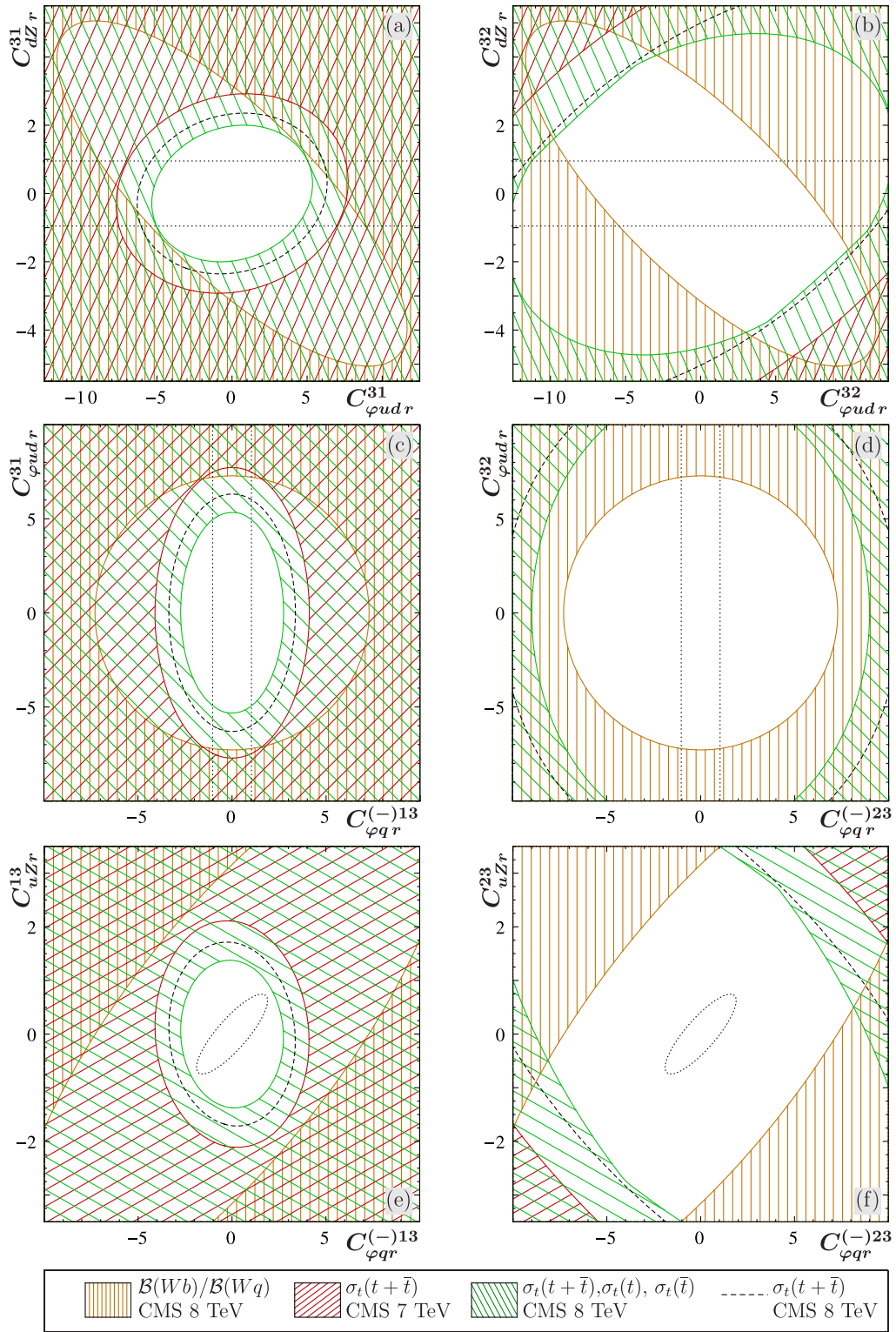


FIG. 7 (color online). Parameter regions for flavor off-diagonal Wtq effective couplings allowed at 95% C.L. Orange hatched area: region excluded by the branching fractions $\text{Br}(Wb)/\sum_i \text{Br}(Wq_i)$ [48] in top decays. Red hatched area: region excluded by the cross section for $pp \rightarrow tq + \bar{t}q$ at 7 TeV [53]. Green hatched area: region excluded by the cross sections for $pp \rightarrow tq + \bar{t}q$, tq , $\bar{t}q$ at 8 TeV [54]. Black dashed line: region excluded by the cross section for $pp \rightarrow tq + \bar{t}q$ at 8 TeV alone [54]. Dotted lines: (a) and (b), bounds on $|C_{dZ}^{3j}|$ ($j = 1, 2$) from (12); (c)–(f), allowed regions from (13).

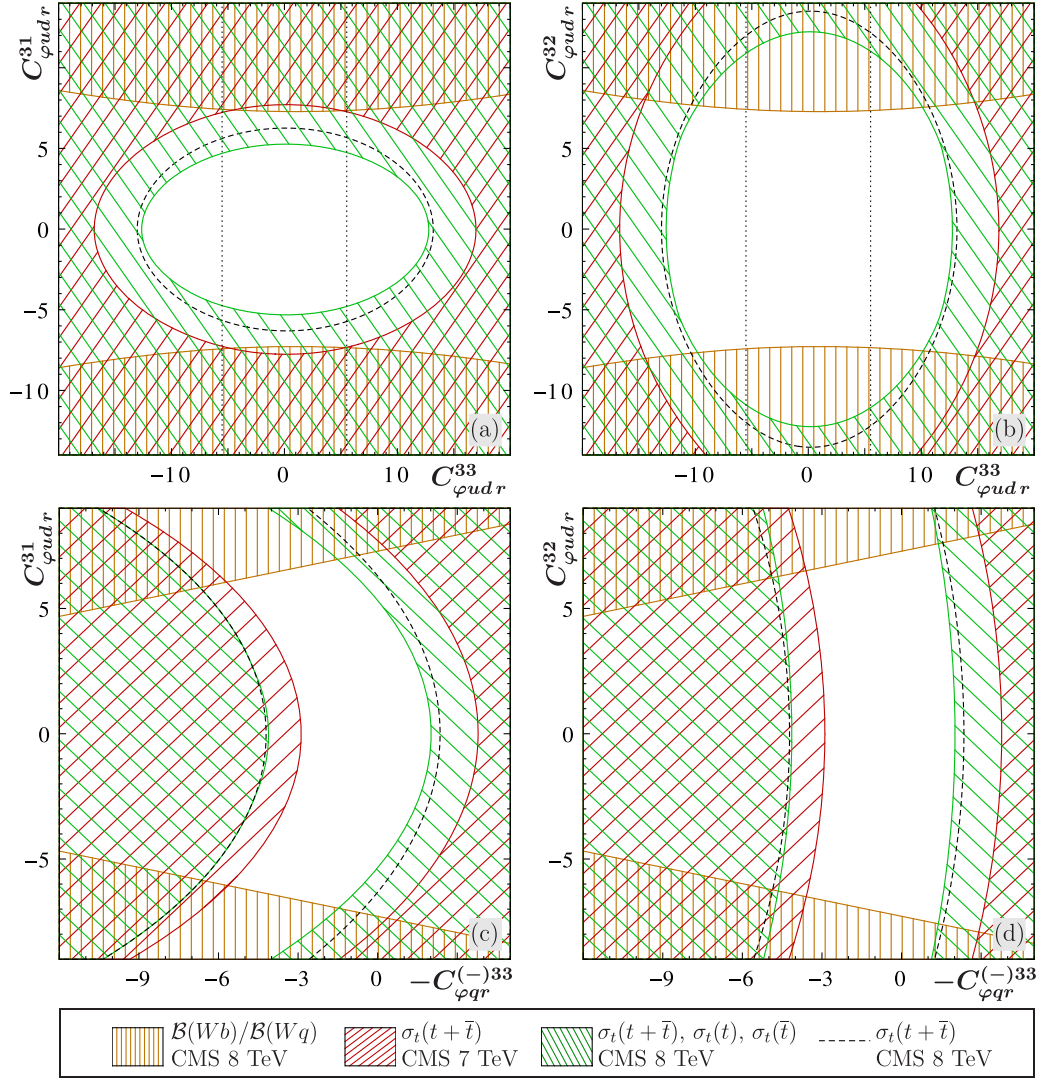


FIG. 8 (color online). Allowed parameter regions at 95% C.L. for the flavor off-diagonal right-handed vector Wtq effective couplings $C_{\varphi ud r}^{3j}$ ($j = 1, 2$) versus flavor-diagonal left- and right-handed vector ones. Color codes as in the previous figure. Black dotted lines in (a) and (b): bounds on $C_{\varphi ud r}^{33}$ from W -helicity fractions in top decays [27].

(orange hatched area). On the other hand, $F_{0,L}$ have a weak dependence on $C_{\varphi q}^{(\pm)33}$, which is bounded by the decay width and single-top production cross sections. The best bounds on $C_{\varphi q}^{(\pm)33}$ are set by the tq production cross sections at 7 TeV (lower bound) and at 8 TeV (upper bound). The intersection of the regions allowed by tq , $\bar{t}q$ and $tq + \bar{t}q$ production at 8 TeV (green hatched areas) is necessarily more restrictive than the region obtained from $tq + \bar{t}q$ production alone, the difference between the two being most apparent for C_{uZ}^{33} and less pronounced in the case of $C_{\varphi q}^{(\pm)33}$.

C. Differential cross sections

Besides the total cross sections for single-top production used in the previous sections, we have considered also the

total and differential cross sections reported by ATLAS for separate and combined single top and antitop production in the LHC at 7 TeV with a total integrated luminosity of 4.58 fb^{-1} .

The effect of these additional data on the allowed parameter regions is illustrated in Fig. 10 for the couplings $C_{\varphi qr}^{(-)33}/C_{uZr}^{33}$. For reference, we include in Fig. 10 the same 95% C.L.-allowed regions as in Fig. 9(e). We combined those CMS cross sections with the total cross sections for $pp \rightarrow tq + \bar{t}q, tq, \bar{t}q$ at 7 TeV measured by ATLAS [55] in a χ^2 analysis, to obtain at 95% C.L. the allowed region shown by the light-blue band in Fig. 10. As seen in the figure, the allowed region is little changed in a neighborhood of the origin by the inclusion of the additional data points.

We further extended the analysis by including all bins in the measured differential cross sections $d\sigma/d|y|(t)$,

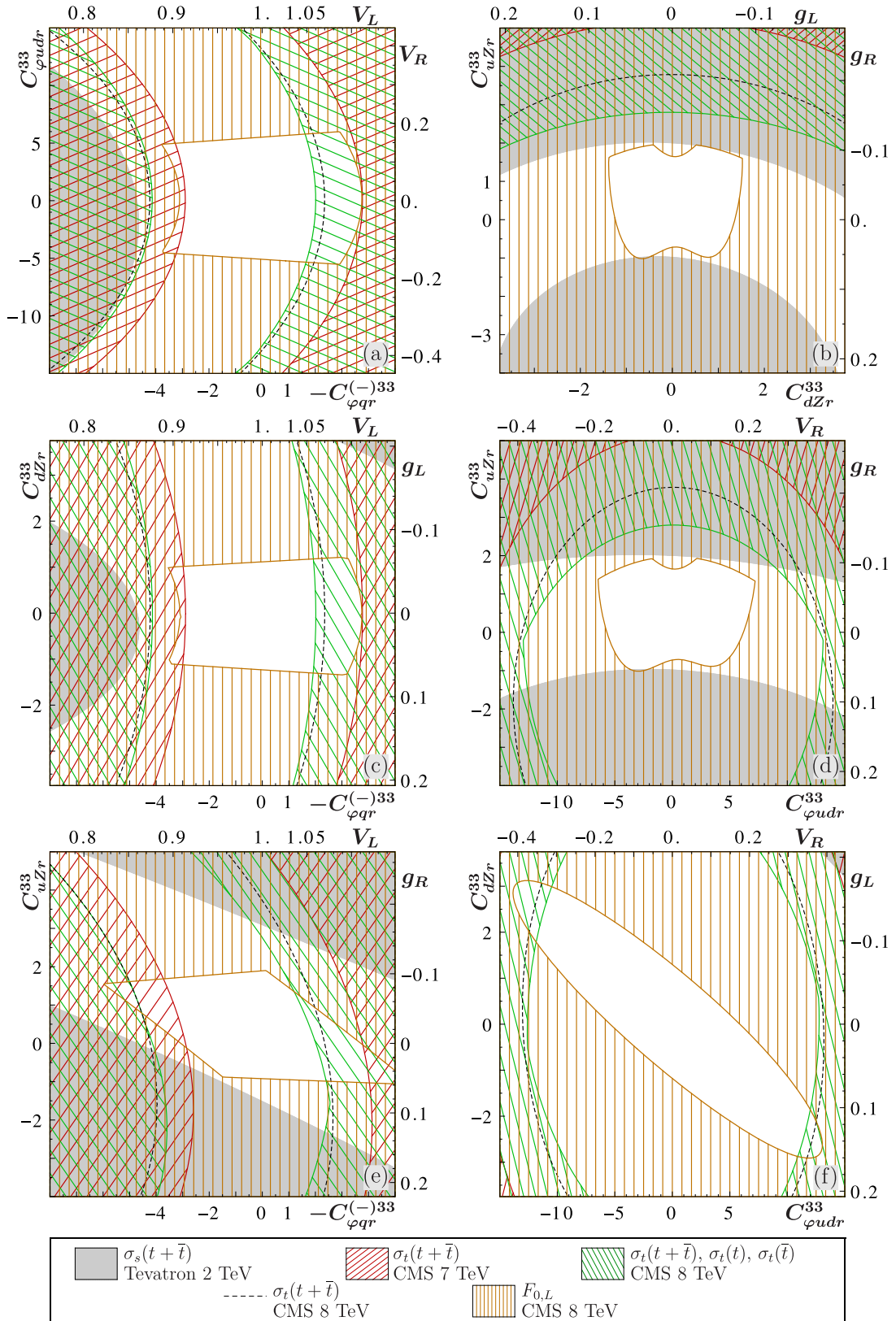


FIG. 9 (color online). Allowed parameter regions at 95% C.L. for flavor-diagonal Wtq effective couplings. Orange hatched area: region excluded by W -helicity fractions in top decays [27] and top decay width [48]. Gray area: region excluded by the cross section for $p\bar{p} \rightarrow i\bar{b} + \bar{t}b$ at 1.96 TeV [77]. Red and green hatched areas and dashed line as in Fig. 7.

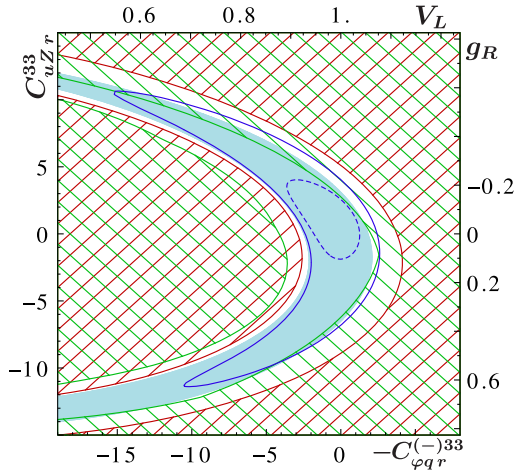


FIG. 10 (color online). Allowed parameter regions at 95% C.L. for two flavor-diagonal Wtq effective couplings. Red and green hatched areas as in previous figures. Light-blue area: allowed region at 95% C.L. determined simultaneously by the total cross sections for $pp \rightarrow tq + \bar{t}q$ at 7 TeV [53], for $pp \rightarrow tq + \bar{t}q$, tq , $\bar{t}q$ at 7 TeV [55], and for $pp \rightarrow tq + \bar{t}q$, tq , $\bar{t}q$ at 8 TeV [54]. Dark-blue solid line: allowed region at 95% C.L. determined simultaneously by the total cross sections and the differential cross sections $d\sigma/d|y|(t)$, $d\sigma/d|y|(\bar{t})$, $d\sigma/d|\vec{p}_T|(t)$, $d\sigma/d|\vec{p}_T|(\bar{t})$, excluding the two highest- $|\vec{p}_T|$ bins. Dark-blue dashed line: allowed region at 95% C.L. determined simultaneously by total and differential cross sections, including all bins.

$d\sigma/d|y|(\bar{t})$ in the χ^2 function, with their correlation matrices, as well as the data for $d\sigma/d|\vec{p}_T|(t)$, $d\sigma/d|\vec{p}_T|(\bar{t})$ excluding the two highest- $|\vec{p}_T|$ bins in each distribution (four excluded bins in total). The resulting allowed region at 95% C.L. is shown in Fig. 10 by the blue solid line. Finally, adding the previously excluded highest- $|\vec{p}_T|$ bins to the χ^2 function, yields the allowed region delimited by the blue dashed line in the figure. As seen there, those highest- $|\vec{p}_T|$ bins have a large effect on the allowed region, which we attribute to the fact that their central values show large deviations ($\sim 2\sigma$) from the SM NLO predictions, especially in the case of $d\sigma/d|\vec{p}_T|(\bar{t})$. We point out as well that the highest- $|\vec{p}_T|$ bin corresponds to an energy range of 150–500 GeV that is relatively close to the new physics scale $\Lambda = 1$ TeV assumed here, which would make the validity of our obtained bounds uncertain.

We conclude that the results from the LHC Run-I (7 TeV) on single-top production do not significantly add to the constraining we have obtained based on Run-II (8 TeV) data. This is true even after considering the input from the absolute rapidity and p_T distributions, unless we take into consideration the large deviations observed in the last two bins.

D. Limits on four-fermion operators

The operators $O_{qq}^{(1,3)ijk}$ with $i, j, k < 3$ contribute to single-top production only through $pp \rightarrow tq$, $t\bar{q}$.

The Feynman diagrams related to these vertices are shown in Fig. 5(a). Due to their flavor off-diagonal nature, there is no interference of these diagrams with the SM ones due to the very small third-generation mixing. Yet, there is an enhanced sensitivity to these couplings because of the large first-generation PDFs. Taking only one coupling to be nonzero at a time, from the single-top production cross section $\sigma(pp \rightarrow tq)$ at 8 TeV [54] we get the following single-coupling bounds. The operators $O_{qq}^{(1,3)1113}$, $O_{qq}^{(1,3)1213}$ receive the strongest bounds among four-quark operators:

$$\begin{aligned} |C_{qq}^{(1)1113}|, |C_{qq}^{(1)1213}| &< 0.30, \\ |C_{qq}^{(3)1113}|, |C_{qq}^{(3)1213}| &< 0.23. \end{aligned} \quad (32)$$

The cross section for antitop production at 8 TeV, and the combined $t + \bar{t}$ production cross sections at 8 and 7 TeV [53,54] lead to somewhat weaker bounds. Similarly, for the analogous four-quark operators involving only one third-generation quark, we obtain the single-coupling bounds:

$$\begin{aligned} |C_{qq}^{(1)1123}| &< 1.23, & |C_{qq}^{(3)1123}| &< 0.50, \\ |C_{qq}^{(1)2113}| &< 0.86, & |C_{qq}^{(3)2113}| &< 0.72. \end{aligned} \quad (33)$$

The operators $O_{qq}^{(1,3)3113}$ and $O_{qq}^{(3)1133}$ contribute to both single-top production channels ($pp \rightarrow tq$, $t\bar{q}$ and $pp \rightarrow t\bar{b}$, $t\bar{b}$) and to $t\bar{t}$ production, while $O_{qq}^{(1)1133}$ contributes only to the latter process. Notice that these four operators are Hermitian, so their couplings are real. The bounds we find are

$$\begin{aligned} -1.07 < C_{qq}^{(1)3113} < 1.19, & -0.80 < C_{qq}^{(3)3113} < 0.96, \\ -2.94 < C_{qq}^{(1)1133} < 2.67, & -0.18 < C_{qq}^{(3)1133} < 0.36. \end{aligned} \quad (34)$$

The bounds on $C_{qq}^{(1)3113}$ result from a combination of the ones obtained from $t\bar{t}$ production ($-1.07 < C_{qq}^{(1)3113} < 1.23$) and those from $t\bar{b}$ production ($-2.19 < C_{qq}^{(1)3113} < 1.19$), both at the Tevatron. As mentioned in Sec. II B, $O_{qq}^{(3)3113} = -O_{qq}^{(1)3113} +$ terms with 0 or 2 top fields, so single-top production does not distinguish between the two. The bounds on $C_{qq}^{(3)3113}$ in (34) arise from $t\bar{t}$ production at the Tevatron. The operator $O_{qq}^{(1)1133}$ does not contribute to single-top production. The limits (34) on $C_{qq}^{(1)1133}$ are a combination of the ones obtained from $t\bar{t}$ production, at 8 TeV at the LHC ($-2.94 < C_{qq}^{(1)1133} < 2.80$) and at the Tevatron ($-3.28 < C_{qq}^{(1)1133} < 2.67$). The tightest limits on $C_{qq}^{(3)1133}$ arise from $t\bar{b}$ production at the Tevatron, the bounds from $t\bar{t}$ production on that coupling being much looser, ~ 3 at 8 TeV and larger at lower energies.

As discussed in Sec. II B, the operator O_{qq}^{1313} contributes to single-top and tt production and $O_{qq}^{3131} = O_{qq}^{1313\dagger}$ to single-top and $\bar{t}\bar{t}$ production. Bounds on $C_{qq}^{(1,3)1313}$ have been given by ATLAS [41] from their measurement of same-sign tt production at 8 TeV. We quote here the ATLAS result for completeness, which in our conventions reads $|C_{qqr}^{(1)1313}|, |C_{qqr}^{(3)1313}| < 0.0265$ at 95% C.L.

The sensitivity of both the tq and tb production processes to the couplings $C_{qq}^{(1)3123}$, $C_{qq}^{(3)1233}$ is significantly enhanced by Cabibbo mixing. The strongest bounds on those couplings arise from tq production at 8 TeV:

$$\begin{aligned} -2.25 < C_{qqr}^{(1)3123} < 2.22, & \quad -2.23 < C_{qqi}^{(1)3123} < 2.23, \\ -1.14 < C_{qqr}^{(3)1233} < 1.09, & \quad -1.11 < C_{qqi}^{(3)1233} < 1.11, \end{aligned} \quad (35)$$

with $tq + \bar{t}q$ production at the same energy leading to somewhat weaker bounds. The operator $O_{qq}^{(3)3123} = -O_{qq}^{(1)3123} + \text{terms with 0 or 2 top fields}$, so the bounds on $C_{qq}^{(3)3123}$ from single-top production are the same as those for $-C_{qq}^{(1)3123}$ in (35). Top pair production is less sensitive than single-top processes to these couplings, leading to bounds about twice as large as those in (35) at 8 TeV and larger at lower energies. For the operator $O_{qq}^{(1)1233}$, which does not contribute to single-top production, the bounds obtained from $\bar{t}\bar{t}$ production at 8 TeV are,

$$-4.72 < C_{qqr}^{(1)1233} < 4.58, \quad -5.18 < C_{qqi}^{(1)1233} < 5.18, \quad (36)$$

significantly weaker than the analogous limits in (35).

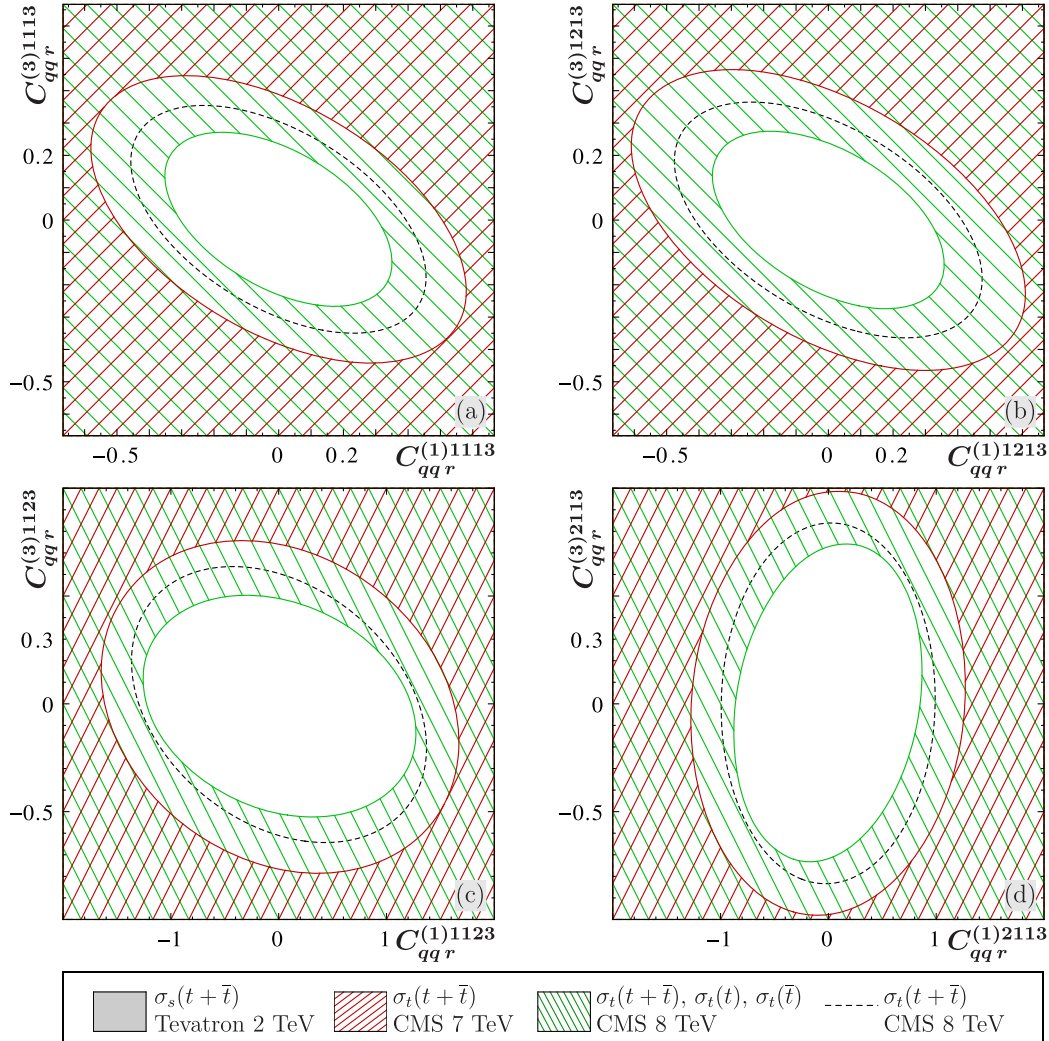


FIG. 11 (color online). Allowed parameter regions at 95% C.L. for contact four-quark effective couplings. Red hatched area: region excluded by the cross section for $pp \rightarrow tq + \bar{t}q$ at 7 TeV [53]. Green hatched area: region excluded by the cross sections for $pp \rightarrow tq + \bar{t}q, tq, \bar{t}q$ at 8 TeV [54]. Black dashed line: region excluded by the cross section for $pp \rightarrow tq + \bar{t}q$ at 8 TeV alone [54]. Gray area: region excluded by the cross section for $p\bar{p} \rightarrow \bar{t}b + \bar{t}b$ at 1.96 TeV [77].

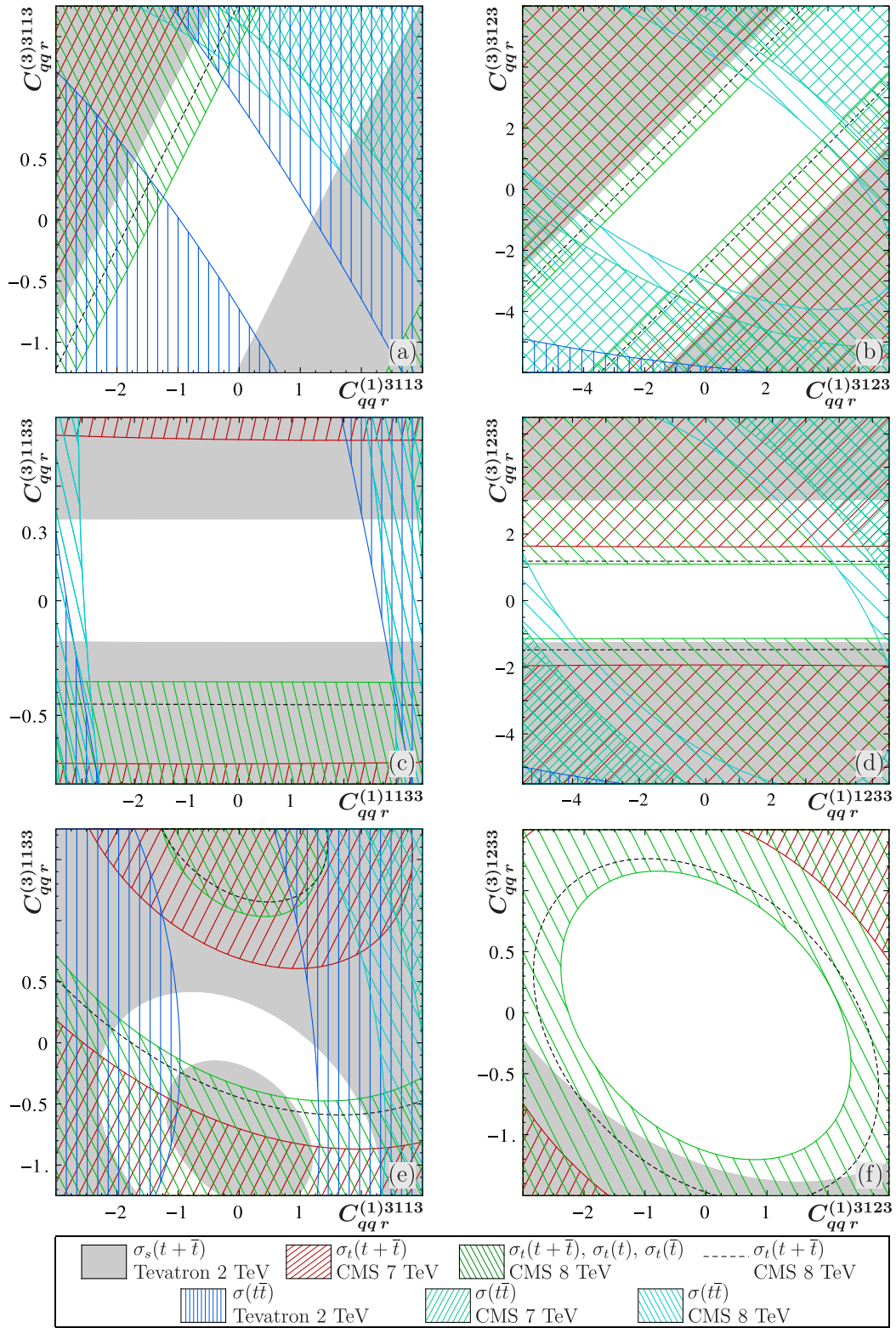


FIG. 12 (color online). Allowed parameter regions at 95% C.L. for contact four-quark effective couplings. Red and green hatched areas, gray area and black dashed line as in the previous figure. Regions excluded by the cross section for $pp \rightarrow t\bar{t}$: blue hatched area (1.96 TeV [68]), light-green hatched area (7 TeV [67]), light-blue hatched area (8 TeV [66]).

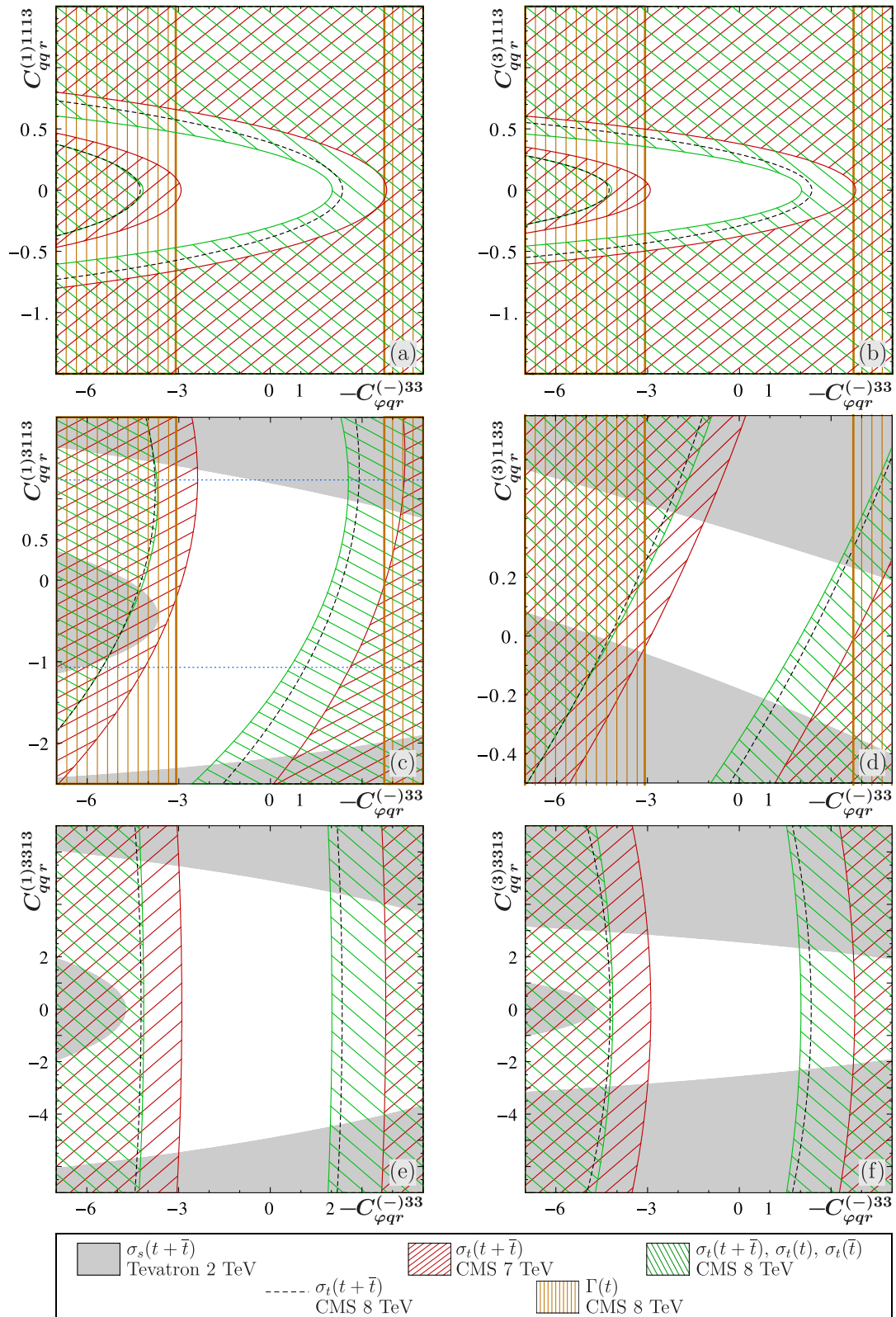


FIG. 13 (color online). Allowed parameter regions at 95% C.L. for four-quark effective couplings versus the flavor-diagonal left-handed vector effective coupling. Red and green hatched areas, gray area and black dashed line as in Fig. 11. Orange hatched area: region excluded by the top decay width [48]. Blue dotted lines: region excluded by the $t\bar{t}$ production cross section at 1.96 TeV [68].

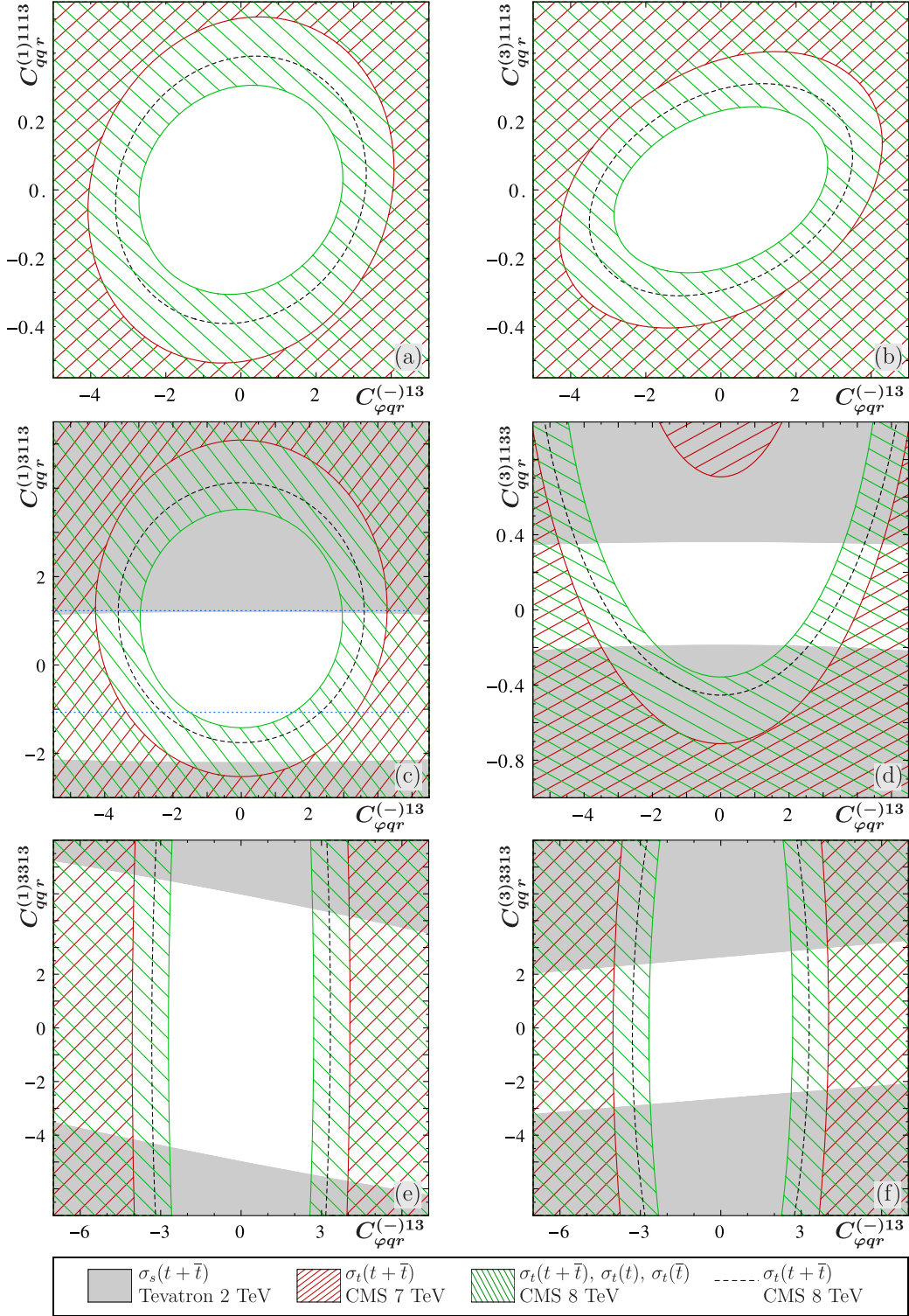


FIG. 14 (color online). Allowed parameter regions at 95% C.L. for four-quark effective couplings versus the flavor off-diagonal left-handed vector effective coupling. Color codes as in Fig. 11. Blue dotted lines: region excluded by the $t\bar{t}$ production cross section at 1.96 TeV [68].

The operators $O_{qq}^{(1)3313}$ and $O_{qq}^{(3)3313}$ also contribute to both tq and tb production. As shown in Fig. 5(c), tq production through these operators involves two b quarks in the initial state, leading to very low sensitivity to these couplings. More

restrictive bounds are furnished by tb production [Fig. 6(b)]. From the cross section measurement at 2 TeV [60] we get,

$$|C_{qq}^{(1)3313}| < 4.92, \quad |C_{qq}^{(3)3313}| < 2.57, \quad (37)$$

Neither production channel, tq or tb , possesses significant sensitivity to $O_{qq}^{(1,3)3323}$.

In Fig. 11 we show allowed regions for four pairs of couplings $C_{qqr}^{(1)ijk3}/C_{qqr}^{(3)ijk3}$ with $i, j, k < 3$. The most restrictive limits for these couplings are set in all cases by the tq production cross section at 8 TeV, with the combined cross section for $tq + \bar{t}q$ yielding slightly weaker bounds. As also seen in the figure, there is sizeable interference between the singlet-singlet and triplet-triplet amplitudes, proportional to $C_{qq}^{(1)}$ and $C_{qq}^{(3)}$, respectively.

Figure 12 displays allowed regions for six pairs of four-quark couplings involving two third-generation quarks. The single-top cross sections do not depend on $C_{qqr}^{(1)31k3} + C_{qqr}^{(3)31k3}$ or on $C_{qqr}^{(1)1k33}$, $k = 1, 2$, as seen in Figs. 12(a)–12(d). The limits in those directions are set by the $t\bar{t}$ production cross section. We remark the fundamental role played by Tevatron data in bounding the couplings involving only first- and third-generation quarks (left column in the figure), whereas those involving one first- and one second-generation quarks (right column in the figure) are bounded by LHC 8 TeV data.

In Fig. 13 we show the allowed regions in the plane of the four-quark couplings C_{qq} involving first-generation quarks and the flavor-diagonal vector coupling $-C_{qqr}^{(-)33}$ (i.e., the parameter V_L). The importance of tb production to bound those couplings involving more than one third-generation quark is apparent from the four lower panels though, as seen in the figure, in the case of $C_{qqr}^{(1)3113}$ more restrictive bounds result from $t\bar{t}$ production.

In Fig. 14 we show the allowed region on the plane of the same four-quark coupling as in the previous figure and the flavor off-diagonal vector coupling $C_{qqr}^{(-)13}$. The interference between the amplitudes proportional to $C_{qq}^{(1,3)1113}$ and those proportional to $C_{qqr}^{(-)13}$, as well as between the amplitudes proportional to $C_{qq}^{(1)3113}$, $C_{qq}^{(3)1133}$ and the SM ones is clearly seen in the figure.

VI. CONCLUSIONS

In this paper we have obtained limits on Wtq vertices in the context of the $SU(2) \times U(1)$ -gauge invariant effective Lagrangian of dimension six. We worked with the basis of operators listed in [28,30], with the operator normalization used in [14,17]. In the SM the Wtq couplings are suppressed by the CKM parameters. No precise direct measurements of V_{td} , V_{ts} exist so far, but there are studies that propose to use single top production distributions in order to achieve higher accuracy [37]. In this study we refer to the Wtq vertices as generated by the dimension six operators. There are previous studies on limits for the diagonal anomalous Wtb coupling based on single top production and W -helicity fractions in the $t \rightarrow bW$ decay, with [7,8,25,26] the most recent references. However, no similar

direct limits have been reported before for the flavor off-diagonal Wts and Wtd couplings. There are 4 independent dimension six operators that give rise to Wtq vertices: $O_{\varphi q}^{(3)k3}$, $O_{\varphi ud}^{3k}$, O_{uW}^{k3} and O_{dW}^{3k} . Three of them generate simultaneously neutral current couplings. Only $O_{\varphi ud}^{3k}$ generates a CC coupling exclusively, which is the right-handed vector $W_\mu^- \bar{d}_R \gamma_\mu t_R$. For the other three operators, we have followed the strategy used in Ref. [14] and we have defined six linear combinations with other three operators $O_{\varphi q}^{(1)k3}$, O_{uB}^{k3} and O_{dB}^{3k} , so as to define separately Ztq_u , Atq_u , Zbq_d and Abq_d interactions, with q_u, q_d any up- or down-type quark.

In order to obtain bounds on these six operators we have considered the FCNC processes $b \rightarrow d\gamma$, $s\gamma$ and $Z \rightarrow bd$, bs , the CC decays $t \rightarrow Wq$ (through its total width, branching fractions and W -helicity fractions) and the single-top production processes $pp \rightarrow tq$ and $p\bar{p} \rightarrow tb$. These results are summarized in Table I and in Figs. 7–8.

For the operators $O_{\varphi q}^{(+)k3}$, O_{dA}^{3k} and O_{dZ}^{3k} ($k = 1, 2$), involving bottom-strange and bottom-down quark interactions, we find that the best bounds are obtained from the LEP measurement of $Z \rightarrow bq$ and the most recent experimental result on the $B \rightarrow X_q \gamma$ decay ($q = d, s$). The direct bounds on these operators are obtained here for the first time.

Notice, however, that for $O_{\varphi q}^{(+)k3}$ there are stronger indirect bounds [45]. We obtain bounds for the operators $O_{\varphi ud}^{3k}$ ($k = 1, 2$), also for the first time. The best bounds on $O_{\varphi ud}^{31}$ result from the single-top production cross section at 8 TeV, and on $O_{\varphi ud}^{32}$ from the ratio of top branching fractions $\text{Br}(t \rightarrow tb)/\sum \text{Br}(t \rightarrow tq)$. We also show in the table and figures, for completeness, the best bounds reported in [14] on $O_{\varphi q}^{(-)k3}$, O_{uZ}^{k3} , from $t \rightarrow jZ$, and on O_{uA}^{k3} from $gq \rightarrow t\gamma$. For the flavor-diagonal effective Wtb coupling we have made an improvement of the previous analyses [7,8,25,26] using the most recent experimental results on W -helicity fractions in top quark decay from $t\bar{t}$ production at the LHC [27].

We have considered also contact-interaction operators involving the top quark, focusing on those four-quark operators related to the Wtq ones by the SM equations of motion. Our results are given in Sec. V D and in Figs. 11–14. The flavor off-diagonal operators $O_{qq}^{(1,3)ijk3}$ (with $ijk = 111$ or a permutation of 112) involving three light quarks and the top are considered here for the first time. The single-top production process $pp \rightarrow tq$ measured at the LHC possesses strong sensitivity to these operators, resulting in the tight bounds on the associated couplings reported above. In fact, the bounds on $C_{qq}^{(1,3)1113}$, $C_{qq}^{(1,3)1213}$ [Eq. (32) and Figs. 11–14] are the strongest ones found in this paper for interactions vertices involving the top quark. The flavor off-diagonal operators $O_{qq}^{(1,3)3313}$ had not been considered before in the literature. For this coupling it is the

single-top process $p\bar{p} \rightarrow tb$ measured at the Tevatron that has some sensitivity, leading to the bounds in Eq. (37). The flavor-diagonal triplet operator $O_{qq}^{(3)1133}$ had already been discussed in [7], though not the singlet $O_{qq}^{(1)3113}$. Both operators lead to interference with the SM, stronger for the triplet operator. The sensitivity to these couplings comes mostly from the Tevatron result for $p\bar{p} \rightarrow tb$ production. Our bounds on $C_{qq}^{(3)1133}$ [Eq. (34) and Figs. 11–14] are somewhat tighter than those reported in [7] for the reasons explained at the end of Sec. IV A.

Single top production at the LHC will mostly have a direct impact on the limits for four-fermion quark operators as well as the flavor-diagonal couplings $C_{\rho q}^{(\pm)33}$ and flavor

off-diagonal $C_{\rho ud}^{3k}$ of top-gauge boson couplings. Also, W -helicity fractions will set strong constraints on the other diagonal Wtb couplings. On the other hand, FCNC processes like $t \rightarrow jZ$ and $pp \rightarrow t\gamma$ [14] at the LHC will be the best options to set strong constraints to the operators that give rise to the off-diagonal $C_{\rho q}^{(-)k3}$, $C_{uZ/A}^{k3}$ and $C_{dZ/A}^{3k}$ couplings.

ACKNOWLEDGMENTS

We acknowledge support from Conacyt and Sistema Nacional de Investigadores de México. We thank Gauthier Durieux and Cen Zhang for useful comments.

-
- [1] F. P. Schilling, Top quark physics at the LHC: A review of the first two years, *Int. J. Mod. Phys. A* **27**, 1230016 (2012); W. Bernreuther and P. Uwer, Top-quark physics at colliders, *Nucl. Part. Phys. Proc.* **261–262**, 414 (2015); J. Blümlein, K. Jansen, M. Krämer, and J. H. Kühn, Proceedings, Advances in Computational Particle Physics: Final Meeting (SFB-TR-9), Durbach, Germany, 2014 (2015); W. Bernreuther, Top quark physics at the LHC, *J. Phys. G* **35**, 083001 (2008); Keynote: Some remarks on top, *Nuovo Cimento Soc. Ital. Fis.* **033C**, 3 (2010); P. Artoisenet *et al.*, A framework for Higgs characterisation, *J. High Energy Phys.* **11** (2013) 043; T. M. P. Tait, Top 2014: Theory summary, [arXiv:1502.07029](https://arxiv.org/abs/1502.07029).
- [2] F. Demartin, F. Maltoni, K. Mawatari, and M. Zaro, Higgs production in association with a single top quark at the LHC, *Eur. Phys. J. C* **75**, 267 (2015); Y. Chen, D. Stolarski, and R. Vega-Morales, Golden probe of the top Yukawa, *Phys. Rev. D* **92**, 053003 (2015); T. Plehn, P. Reimitz, and T. Schell, Measuring the Top Yukawa Coupling at 100 TeV, [arXiv:1507.08169](https://arxiv.org/abs/1507.08169); K. Kolodziej and A. Slapik, Probing the top-Higgs coupling through the secondary lepton distributions in the associated production of the top-quark pair and Higgs boson at the LHC, *Eur. Phys. J. C* **75**, 475 (2015); D. Barducci, S. De Curtis, S. Moretti, and G. M. Pruna, Top pair production at a future e^+e^- machine in a composite Higgs scenario, *J. High Energy Phys.* **08** (2015) 127; M. R. Buckley and D. Goncalves, Boosting the direct CP measurement of the Higgs-top coupling, [arXiv:1507.07926](https://arxiv.org/abs/1507.07926); J. Yue, Enhanced thj signal at the LHC with $h \rightarrow \gamma\gamma$ decay and \mathcal{CP} -violating top-Higgs coupling, *Phys. Lett. B* **744**, 131 (2015).
- [3] A. O. Bouzas and F. Larios, Electromagnetic dipole moments of the top quark, *Phys. Rev. D* **87**, 074015 (2013); Probing tt and ttZ couplings at the LHeC, *Phys. Rev. D* **88**, 094007 (2013).
- [4] U. Baur, A. Juste, L. H. Orr, and D. Rainwater, Probing electroweak top quark couplings at hadron and lepton colliders, *Nucl. Phys. B, Proc. Suppl.* **160**, 17 (2006); Probing electroweak top quark couplings at hadron colliders, *Phys. Rev. D* **71**, 054013 (2005); U. Baur, M. Buice, and L. H. Orr, Direct measurement of the top quark charge at hadron colliders, *Phys. Rev. D* **64**, 094019 (2001); L. Labun and J. Rafelski, Top anomalous magnetic moment and the two photon decay of Higgs boson, *Phys. Rev. D* **88**, 071301 (2013); A. Cordero-Cid, J. M. Hernandez, G. Tavares-Velasco, and J. J. Toscano, Bounding the top and bottom electric dipole moments from neutron experimental data, *J. Phys. G* **35**, 025004 (2008); R. Martinez and J. A. Rodriguez, Constraint of the magnetic moment of the top quark from $R(b)$, *Phys. Rev. D* **60**, 077504 (1999).
- [5] J. Brod, A. Greljo, E. Stamou, and P. Uttayarat, Probing anomalous $t\bar{t}Z$ interactions with rare meson decays, *J. High Energy Phys.* **02** (2015) 141; R. Rötsch and M. Schulze, Probing top-Z dipole moments at the LHC and ILC, *J. High Energy Phys.* **08** (2015) 044; Constraining couplings of top quarks to the Z boson in $(t\bar{t}) + Z$ production at the LHC, *J. High Energy Phys.* **07** (2014) 091; F. Richard, Can LHC observe an anomaly in $t\bar{t}Z$ production?, [arXiv:1304.3594](https://arxiv.org/abs/1304.3594); F. Larios, E. Malkawi, and C. P. Yuan, Probing the electroweak symmetry breaking sector with the top quark, *Acta Phys. Pol. B* **27**, 3741 (1996); P. Janot, Top-quark electroweak couplings at the FCC-ee, *J. High Energy Phys.* **04** (2015) 182.
- [6] D. Buarque Franzosi and C. Zhang, Probing the top-quark chromomagnetic dipole moment at next-to-leading order in QCD, *Phys. Rev. D* **91**, 114010 (2015); J. F. Kamenik, M. Papucci, and A. Weiler, Constraining the dipole moments of the top quark, *Phys. Rev. D* **85**, 071501 (2012); **88**, 039903 (E) (2013); K. Kumar, T. M. P. Tait, and R. Vega-Morales, Manifestations of top compositeness at colliders, *J. High Energy Phys.* **05** (2009) 022; R. Martinez, M. A. Perez, and N. Poveda, Chromomagnetic dipole moment of the top quark revisited, *Eur. Phys. J. C* **53**, 221 (2008); Z. Hioki and K. Ohkuma, Latest constraint on nonstandard top-gluon couplings at hadron colliders and its future prospect, *Phys. Rev. D* **88**, 017503 (2013); Q. H. Cao, C. R. Chen, F. Larios, and C.-P. Yuan, Anomalous gtt couplings in the lightest Higgs model with T-parity, *Phys. Rev. D* **79**, 015004 (2009); L. Labun and J. Rafelski, Higgs two-gluon decay and the

- top-quark chromomagnetic moment, [arXiv:1210.3150](#); J. L. Diaz-Cruz, M. A. Perez, and J. J. Toscano, Tests of Higgs and top effective interactions, *Phys. Lett. B* **398**, 347 (1997); B. Lillie, J. Shu, and T. M. P. Tait, Top Compositeness at the Tevatron and LHC, *J. High Energy Phys.* **04** (2008) 087.
- [7] M. Fabbrichesi, M. Pinamonti, and A. Tonero, Limits on anomalous top quark gauge couplings from Tevatron and LHC data, *Eur. Phys. J. C* **74**, 3193 (2014).
- [8] C. Bernardo, N. F. Castro, M. C. N. Fiolhais, H. Goncalves, A. G. C. Guerra, M. Oliveira, and A. Onofre, Studying the Wtb vertex structure using recent LHC results, *Phys. Rev. D* **90**, 113007 (2014).
- [9] F. Bach and T. Ohl, Anomalous top couplings at hadron colliders revisited, *Phys. Rev. D* **86**, 114026 (2012).
- [10] Q. H. Cao and B. Yan, Determining V_{tb} at electron-positron colliders, *Phys. Rev. D* **92**, 094018 (2015); E. L. Berger, Q. H. Cao, and I. Low, Model independent constraints among the Wtb , Zb anti- b , and Zt anti- t couplings, *Phys. Rev. D* **80**, 074020 (2009); F. Larios and M. A. Perez, New physics effects on hadronic decay asymmetries of the top quark, *Phys. Rev. D* **85**, 017503 (2012); I. T. Cakir, A. Senol, and A. T. Tasci, Associated production of single top quark and W -boson through anomalous couplings at LHeC based γp colliders, *Mod. Phys. Lett. A* **29**, 1450021 (2014); S. Dutta, A. Goyal, M. Kumar, and B. Mellado, Measuring anomalous Wtb couplings at e^-p collider, [arXiv:1307.1688](#); B. Sahin and A. A. Billur, Anomalous Wtb couplings in gamma-proton collision at the LHC, *Phys. Rev. D* **86**, 074026 (2012); Q. H. Cao, J. Wudka, and C.-P. Yuan, Search for new physics via single top production at the LHC, *Phys. Lett. B* **658**, 50 (2007); A. Avilez-Lopez, H. Novales-Sanchez, G. Tavares-Velasco, and J. J. Toscano, Bound on the anomalous tbW coupling from two-loop contribution to neutron electric dipole moment, *Phys. Lett. B* **653**, 241 (2007); P. Batra and T. M. P. Tait, Measuring the W - t - b Interaction at the ILC, *Phys. Rev. D* **74**, 054021 (2006); J. A. Aguilar-Saavedra, J. Carvalho, N. F. Castro, A. Onofre, and F. Veloso, ATLAS sensitivity to Wtb anomalous couplings in top quark decays, *Eur. Phys. J. C* **53**, 689 (2008); Q. H. Cao and J. Wudka, Search for new physics via single top production at TeV energy $e\gamma$ colliders, *Phys. Rev. D* **74**, 094015 (2006).
- [11] F. Bach and T. Ohl, Anomalous top charged-current contact interactions in single top production at the LHC, *Phys. Rev. D* **90**, 074022 (2014). See also, J. Gao, C. S. Li, and C. P. Yuan, NLO QCD corrections to dijet production via quark contact interactions, *J. High Energy Phys.* **07** (2012) 037.
- [12] I. A. Sarmiento-Alvarado, A. O. Bouzas, and F. Larios, Analysis of top-quark charged-current coupling at the LHeC, *J. Phys. G* **42**, 085001 (2015).
- [13] C. R. Chen, Searching for new physics with triple-top signal at the LHC, *Phys. Lett. B* **736**, 321 (2014).
- [14] G. Durieux, F. Maltoni, and C. Zhang, Global approach to top-quark flavor-changing interactions, *Phys. Rev. D* **91**, 074017 (2015).
- [15] R. A. Coimbra, P. M. Ferreira, R. B. Guedes, O. Oliveira, A. Onofre, R. Santos, and M. Won, Dimension six FCNC operators and top production at the LHC, *Phys. Rev. D* **79**, 014006 (2009).
- [16] J. J. Zhang, C. S. Li, J. Gao, H. Zhang, Z. Li, C.-P. Yuan, and T. C. Yuan, Next-to-Leading Order QCD Corrections to the Top Quark Decay via Model-Independent FCNC Couplings, *Phys. Rev. Lett.* **102**, 072001 (2009); J. L. Diaz-Cruz, R. Martinez, M. A. Perez, and A. Rosado, Flavor changing radiative decay of the t quark, *Phys. Rev. D* **41**, 891 (1990); F. Larios, R. Martinez, and M. A. Perez, New physics effects in the flavor-changing neutral couplings of the top quark, *Int. J. Mod. Phys. A* **21**, 3473 (2006) J. Drobnak, S. Fajfer, and J. F. Kamenik, QCD corrections to flavor changing neutral coupling mediated rare top quark decays, *Phys. Rev. D* **82**, 073016 (2010). F. Larios and F. Penunuri, FCNC production of same sign top quark pairs at the LHC, *J. Phys. G* **30**, 895 (2004); N. Kidonakis and A. Belyaev, FCNC top quark production via anomalous tqV couplings beyond leading order, *J. High Energy Phys.* **12** (2003) 004; D. Atwood, S. K. Gupta, and A. Soni, Same-sign tops: A powerful diagnostic test for models of new physics, *J. High Energy Phys.* **04** (2013) 035; J. L. Diaz-Cruz, M. A. Perez, G. Tavares-Velasco, and J. J. Toscano, Testing flavor-changing neutral currents in the rare top quark decays $t \rightarrow cV_iV_j$, *Phys. Rev. D* **60**, 115014 (1999); G. A. Gonzalez-Sprinberg, R. Martinez, and J. A. Rodriguez, FCNC top quark decays in extra dimensions, *Eur. Phys. J. C* **51**, 919 (2007).
- [17] C. Zhang, Effective field theory approach to top-quark decay at next-to-leading order in QCD, *Phys. Rev. D* **90**, 014008 (2014).
- [18] J. J. Zhang, C. S. Li, J. Gao, H. X. Zhu, C.-P. Yuan, and T. C. Yuan, Next-to-leading order QCD corrections to the top quark decay via the flavor-changing neutral-current operators with mixing effects, *Phys. Rev. D* **82**, 073005 (2010).
- [19] J. Drobnak, S. Fajfer, and J. F. Kamenik, Flavor Changing Neutral Coupling Mediated Radiative Top Quark Decays at Next-to-Leading Order in QCD, *Phys. Rev. Lett.* **104**, 252001 (2010); QCD Corrections to Flavor Changing Neutral Coupling Mediated Rare Top Quark Decays, *Phys. Rev. D* **82**, 073016 (2010).
- [20] G. Tetlalmatzi, J. G. Contreras, F. Larios, and M. A. Perez, Higgs boson flavor-changing neutral coupling and $h \rightarrow t^*c$ decay at a muon collider, *Phys. Rev. D* **81**, 037303 (2010); J. L. Diaz-Cruz, From the Higgs to the top: Couplings and rare decays, [arXiv:1505.00757](#); A. Fernandez, C. Pagliarone, F. Ramirez-Zavaleta, and J. J. Toscano, Higgs mediated double flavor violating top decays in effective theories, *J. Phys. G* **37**, 085007 (2010); A. Cordero-Cid, M. A. Perez, G. Tavares-Velasco, and J. J. Toscano, Effective Lagrangian approach to Higgs-mediated FCNC top quark decays, *Phys. Rev. D* **70**, 074003 (2004); H. Hesari, H. Khanpour, and M. M. Najafabadi, Direct and indirect searches for top-Higgs FCNC couplings, [arXiv:1508.07579](#); L. Wu, Enhancing thj production from top-Higgs FCNC couplings, *J. High Energy Phys.* **02** (2015) 061; A. Dery, A. Efrati, Y. Nir, Y. Soreq, and V. Susi, Model building for flavor changing Higgs couplings, *Phys. Rev. D* **90**, 115022 (2014).
- [21] H. Sun, Probe anomalous tq couplings through single top photoproduction at the LHC, *Nucl. Phys.* **B886**, 691 (2014); F. Larios, F. Penunuri, and M. A. Perez, Top-pions and single top production at HERA and THERA, *Phys. Lett. B* **605**, 301 (2005); X. Q. Li, Y. D. Yang, and X. B. Yuan,

- Anomalous $tq\gamma$ coupling effects in exclusive radiative B-meson decays, *J. High Energy Phys.* **08** (2011) 075; R. Martinez, M. A. Perez, and J. J. Toscano, Implications of $b \rightarrow s\gamma$ on the anomalous electromagnetic couplings of gauge bosons and quarks, *Phys. Lett. B* **340**, 91 (1994).
- [22] H. Gong, Y. D. Yang, and X. B. Yuan, Constraints on anomalous tcZ coupling from $\bar{B} \rightarrow \bar{K}^*\mu^+\mu^-$ and $B_s \rightarrow \mu^+\mu^-$ decays, *J. High Energy Phys.* **05** (2013) 062; X. Q. Li, Y. D. Yang, and X. B. Yuan, Anomalous tqZ coupling effects in rare B- and K-meson decays, *J. High Energy Phys.* **03** (2012) 018; J. Campbell, R. K. Ellis, and R. Rntsch, Single top production in association with a Z boson at the LHC, *Phys. Rev. D* **87**, 114006 (2013).
- [23] N. Kidonakis and E. Martin, Soft-gluon corrections in FCNC top-quark production via anomalous gluon couplings, *Phys. Rev. D* **90**, 054021 (2014); T. M. P. Tait and C. P. Yuan, Anomalous $t-c-g$ coupling: The connection between single top production and top decay, *Phys. Rev. D* **55**, 7300 (1997); S. M. Etesami and M. Mohammadi Najafabadi, Study of anomalous top quark FCNC interactions via tW -channel of single top, *Phys. Rev. D* **81**, 117502 (2010); G. Eilam, M. Frank, and I. Turan, Single top production via gluon fusion at LHC, *Phys. Rev. D* **74**, 035012 (2006); R. Guedes, R. Santos, and M. Won, Limits on strong flavor changing neutral current top couplings at the LHC, *Phys. Rev. D* **88**, 114011 (2013); P. M. Ferreira and R. Santos, Strong flavor changing effective operator contributions to single top quark production, *Phys. Rev. D* **73**, 054025 (2006); P. M. Ferreira, O. Oliveira, and R. Santos, Flavor changing strong interaction effects on top quark physics at the LHC, *Phys. Rev. D* **73**, 034011 (2006); P. M. Ferreira, R. B. Guedes, and R. Santos, Combined effects of strong and electroweak FCNC effective operators in top quark physics at the CERN LHC, *Phys. Rev. D* **77**, 114008 (2008); C. X. Yue, J. Wang, Y. Yu, and T. T. Zhang, The anomalous top quark coupling tqg and tW production at the LHC, *Phys. Lett. B* **705**, 222 (2011).
- [24] S. Faller, S. Gadatsch, and T. Mannel, Minimal flavor violation and anomalous top decays, *Phys. Rev. D* **88**, 035006 (2013).
- [25] Q. H. Cao, B. Yan, J. H. Yu, and C. Zhang, A general analysis of Wtb anomalous couplings, [arXiv:1504.03785](https://arxiv.org/abs/1504.03785).
- [26] A. Buckley, C. Englert, J. Ferrando, D. J. Miller, L. Moore, M. Russell, and C. D. White, A global fit of top quark effective theory to data, [arXiv:1506.08845](https://arxiv.org/abs/1506.08845).
- [27] CMS Collaboration, CMS Physics Analysis Summary Report No. TOP-14-017.
- [28] J. A. Aguilar-Saavedra, A minimal set of top anomalous couplings, *Nucl. Phys.* **B812**, 181 (2009).
- [29] J. A. Aguilar-Saavedra, Effective four-fermion operators in top physics: A roadmap, *Nucl. Phys.* **B843**, 638 (2011); **B851**, 443(E) (2011).
- [30] B. Grzadkowski, M. Iskrzynski, M. Misiak, and J. Rosiek, Dimension-six terms in the standard model Lagrangian, *J. High Energy Phys.* **10** (2010) 085.
- [31] J. Alwall, R. Frederix, S. Frixione, V. Hirschi, F. Maltoni, O. Mattelaer, H.-S. Shao, T. Stelzer, P. Torrielli, and M. Zaro, The automated computation of tree-level and next-to-leading order differential cross sections, and their matching to parton shower simulations, *J. High Energy Phys.* **07** (2014) 079.
- [32] J. F. Kamenik, J. Shu, and J. Zupan, Review of new physics effects in t-tbar production, *Eur. Phys. J. C* **72**, 2102 (2012); C. Degrande, J. M. Gerard, C. Grojean, F. Maltoni, and G. Servant, An effective approach to same sign top pair production at the LHC and the forward-backward asymmetry at the Tevatron, *Phys. Lett. B* **703**, 306 (2011); Probing top-Higgs non-standard interactions at the LHC, *J. High Energy Phys.* **07** (2012) 036; **03** (2013) 032(E); E. L. Berger, Q. H. Cao, and I. Low, Model independent constraints among the Wtb , Zb anti- b , and Zt anti- t couplings, *Phys. Rev. D* **80**, 074020 (2009); T. Han, Z. Liu, Z. Qian, and J. Sayre, Improving Higgs coupling measurements through ZZ fusion at the ILC, *Phys. Rev. D* **91**, 113007 (2015); P. Artoisenet *et al.*, A framework for Higgs characterisation, *J. High Energy Phys.* **11** (2013) 043; F. Demartin, F. Maltoni, K. Mawatari, and M. Zaro, Higgs production in association with a single top quark at the LHC, *Eur. Phys. J. C* **75**, 267 (2015).
- [33] C. Degrande, N. Greiner, W. Kilian, O. Mattelaer, H. Mebane, T. Stelzer, S. Willenbrock, and C. Zhang, Effective field theory: A modern approach to anomalous couplings, *Ann. Phys. (N.Y.)* **335**, 21 (2013); C. Zhang, N. Greiner, and S. Willenbrock, Constraints on non-standard top quark couplings, *Phys. Rev. D* **86**, 014024 (2012); C. Zhang and S. Willenbrock, Effective-field-theory approach to top-quark production and decay, *Phys. Rev. D* **83**, 034006 (2011).
- [34] S. Willenbrock and C. Zhang, Effective field theory beyond the standard model, *Annu. Rev. Nucl. Part. Sci.* **64**, 83 (2014); L. Berthier and M. Trott, Towards consistent electroweak precision data constraints in the SMEFT, *J. High Energy Phys.* **05** (2015) 024; J. Ellis, V. Sanz, and T. You, The effective standard model after LHC Run I, *J. High Energy Phys.* **03** (2015) 157; R. Alonso, H. M. Chang, E. E. Jenkins, A. V. Manohar, and B. Shotwell, Renormalization group evolution of dimension-six baryon number violating operators, *Phys. Lett. B* **734**, 302 (2014); R. Alonso, E. E. Jenkins, A. V. Manohar, and M. Trott, Renormalization group evolution of the standard model dimension six operators III: Gauge coupling dependence and phenomenology, *J. High Energy Phys.* **04** (2014) 159; E. E. Jenkins, A. V. Manohar, and M. Trott, Renormalization group evolution of the standard model dimension six operators II: Yukawa dependence, *J. High Energy Phys.* **01** (2014) 035; E. E. Jenkins, A. V. Manohar, and M. Trott, Renormalization group evolution of the standard model dimension six operators I: Formalism and lambda dependence, *J. High Energy Phys.* **10** (2013) 087; J. Elias-Mir, J. R. Espinosa, E. Masso, and A. Pomarol, Renormalization of dimension-six operators relevant for the Higgs decays $h \rightarrow \gamma\gamma$, γZ , *J. High Energy Phys.* **08** (2013) 033; J. Elias-Miro, C. Grojean, R. S. Gupta, and D. Marzocca, Scaling and tuning of EW and Higgs observables, *J. High Energy Phys.* **05** (2014) 019.
- [35] W. Buchmueller and D. Wyler, Effective Lagrangian analysis of new interactions and flavor conservation, *Nucl. Phys.* **B268**, 621 (1986).

- [36] B. Grzadkowski, Z. Hioki, K. Ohkuma, and J. Wudka, Probing anomalous top quark couplings induced by dimension-six operators at photon colliders, *Nucl. Phys.* **B689**, 108 (2004).
- [37] J. A. Aguilar-Saavedra and A. Onofre, Using single top rapidity to measure V_{td} , V_{ts} , V_{tb} at hadron colliders, *Phys. Rev. D* **83**, 073003 (2011); A. Ali, F. Barreiro, and T. Lagouri, Prospects of measuring the CKM matrix element $|V_{ts}|$ at the LHC, *Phys. Lett. B* **693**, 44 (2010); T. Lagouri, Prospects of direct determination of $|V_{tq}|$ CKM matrix elements at the LHC, [arXiv:1212.0013](https://arxiv.org/abs/1212.0013); H. Lacker, A. Menzel, F. Spettel, D. Hirschbuhl, J. Luck, F. Maltoni, W. Wagner, and M. Zaro, Model-independent extraction of $|V_{tq}|$ matrix elements from top-quark measurements at hadron colliders, *Eur. Phys. J. C* **72**, 2048 (2012).
- [38] J. A. Aguilar-Saavedra and J. Bernabeu, W polarisation beyond helicity fractions in top quark decays, *Nucl. Phys.* **B840**, 349 (2010); J. A. Aguilar-Saavedra, N. F. Castro, and A. Onofre, Constraints on the Wtb vertex from early LHC data, *Phys. Rev. D* **83**, 117301 (2011).
- [39] V. Khachatryan *et al.* (CMS Collaboration), Measurement of the W boson helicity in events with a single reconstructed top quark in pp collisions at $\sqrt{s} = 8$ TeV, *J. High Energy Phys.* **01** (2015) 053.
- [40] C.-R. Chen, F. Larios, and C.-P. Yuan, General analysis of single top production and W helicity in top decay, *Phys. Lett. B* **631**, 126 (2005).
- [41] (ATLAS Collaboration), Analysis of events with b -jets and a pair of leptons of the same charge in pp collisions at $\sqrt{s} = 8$ TeV with the ATLAS detector, *J. High Energy Phys.* **10** (2015) 150.
- [42] T. Hurth, E. Lunghi, and W. Porod, Untagged $\bar{B} \rightarrow X_{s+d\gamma}$ CP asymmetry as a probe for new physics, *Nucl. Phys.* **B704**, 56 (2005).
- [43] Y. Amhis *et al.* (Heavy Flavor Averaging Group (HFAG) Collaboration), Averages of b -hadron, c -hadron, and τ -lepton properties as of summer 2014, [arXiv:1412.7515](https://arxiv.org/abs/1412.7515).
- [44] J. Fuster, F. Martinez-Vidal, and P. Tortosa (DELPHI Collaboration), Reports No. CERN-OPEN-99-393, No. CERN-DELPHI-99-81.
- [45] A. Efrati, A. Falkowski, and Y. Soreq, Electroweak constraints on flavorful effective theories, *J. High Energy Phys.* **07** (2015) 018.
- [46] S. Chatrchyan *et al.* (CMS Collaboration), Search for Flavor-Changing Neutral Currents in Top-Quark Decays $t \rightarrow Zq$ in pp Collisions at $\sqrt{s} = 8$ TeV, *Phys. Rev. Lett.* **112**, 171802 (2014); G. Aad *et al.* (ATLAS Collaboration), Search for flavour-changing neutral current top-quark decays to qZ in pp collision data collected with the ATLAS detector at $\sqrt{s} = 8$ TeV, [arXiv:1508.05796](https://arxiv.org/abs/1508.05796).
- [47] J. L. Diaz-Cruz, R. Gaitan-Lozano, G. Lopez-Castro, and C. E. Pagliarone, CKM-suppressed top quark decays $t \rightarrow s(d) + W$ in the standard model and beyond, *Phys. Rev. D* **77**, 094010 (2008).
- [48] V. Khachatryan *et al.* (CMS Collaboration), Measurement of the ratio $B(t \rightarrow Wb)/B(t \rightarrow Wq)$ in pp collisions at $\sqrt{s} = 8$ TeV, *Phys. Lett. B* **736**, 33 (2014).
- [49] A. Czarnecki, J. G. Korner, and J. H. Piclum, Helicity fractions of W bosons from top quark decays at NNLO in QCD, *Phys. Rev. D* **81**, 111503 (2010).
- [50] J. Drobnak, S. Fajfer, and J. F. Kamenik, New physics in $t \rightarrow bW$ decay at next-to-leading order in QCD, *Phys. Rev. D* **82**, 114008 (2010).
- [51] (CDF Collaboration), Measurement of $R = \mathcal{B}(t \rightarrow Wb)/\mathcal{B}(t \rightarrow Wq)$ in top-quark-pair decays using lepton + jets events and the full CDF run II dataset, *Phys. Rev. D* **87**, 111101(R) (2013).
- [52] (D0 Collaboration), Precision Measurement of the Ratio $\mathcal{B}(t \rightarrow Wb)/\mathcal{B}(t \rightarrow Wq)$ and Extraction of V_{tb} , *Phys. Rev. Lett.* **107**, 121802 (2011).
- [53] S. Chatrchyan *et al.* (CMS Collaboration), Measurement of the single-top-quark t -channel cross section in pp collisions at $\sqrt{s} = 7$ TeV, *J. High Energy Phys.* **12** (2012) 035.
- [54] V. Khachatryan *et al.* (CMS Collaboration), Measurement of the t -channel single-top-quark production cross section and of the $|V_{tb}|$ CKM matrix element in pp collisions at $\sqrt{s} = 8$ TeV, *J. High Energy Phys.* **06** (2014) 090.
- [55] (ATLAS Collaboration), Comprehensive measurements t -channel single top-quark of production cross sections at $\sqrt{s} = 7$ TeV with the ATLAS detector, *Phys. Rev. D* **90**, 112006 (2014).
- [56] N. Kidonakis, Top quark production, [arXiv:1311.0283](https://arxiv.org/abs/1311.0283). See also, Next-to-next-to-leading-order collinear and soft gluon corrections for t -channel single top quark production, *Phys. Rev. D* **83**, 091503 (2011).
- [57] N. Kidonakis, Next-to-next-to-leading soft-gluon corrections for the top quark cross section and transverse momentum distribution, *Phys. Rev. D* **82**, 114030 (2010).
- [58] N. Kidonakis, Next-to-next-to-leading logarithm resummation for s -channel single top quark production, *Phys. Rev. D* **81**, 054028 (2010).
- [59] N. Kidonakis, Top quark production, [arXiv:1311.0283](https://arxiv.org/abs/1311.0283).
- [60] T. Aaltonen *et al.* (CDF and D0 Collaborations), Observation of s -Channel Production of Single Top Quarks at the Tevatron, *Phys. Rev. Lett.* **112**, 231803 (2014).
- [61] (ATLAS Collaboration), Search for s -channel single top-quark production in proton-proton collisions at $\sqrt{s} = 8$ TeV with the ATLAS detector, *Phys. Lett. B* **740**, 118 (2015).
- [62] (CMS Collaboration), CMS Physics Analysis Summary Report No. TOP-13-009.
- [63] S. Chatrchyan *et al.* (CMS Collaboration), Evidence for Associated Production of a Single Top Quark and W Boson in pp Collisions at $\sqrt{s} = 7$ TeV, *Phys. Rev. Lett.* **110**, 022003 (2013).
- [64] S. Chatrchyan *et al.* (CMS Collaboration), Observation of the Associated Production of Single Top Quark and a W Boson in pp Collisions at $\sqrt{s} = 8$ TeV, *Phys. Rev. Lett.* **112**, 231802 (2014).
- [65] N. Kidonakis, Two-loop soft anomalous dimensions for single top quark associated production with a W^- or H^- , *Phys. Rev. D* **82**, 054018 (2010).
- [66] (CMS Collaboration), Measurement of the $t\bar{t}$ production cross section in the dilepton channel in pp collisions at $\sqrt{s} = 8$ TeV, *J. High Energy Phys.* **02** (2014) 024.
- [67] (CMS Collaboration), Measurement of the $t\bar{t}$ production cross section in pp collisions at $\sqrt{s} = 7$ TeV with lepton + jets final states, *Phys. Lett. B* **720**, 83 (2013).

- [68] (CDF and D0 Collaborations), Combination of measurements of the top-quark pair production cross section from the Tevatron Collider, *Phys. Rev. D* **89**, 072001 (2014).
- [69] M. Czakon and A. Mitov, Top++, a program for the calculation of the top-pair cross-section at hadron colliders, *Comput. Phys. Commun.* **185**, 2930 (2014).
- [70] M. Czakon, P. Fiedler, and A. Mitov, The Total Top Quark Pair Production Cross Section at Hadron Colliders through $O(\alpha_S^4)$, *Phys. Rev. Lett.* **110**, 252004 (2013).
- [71] V. Ahrens, A. Ferroglia, M. Neubert, B. D. Pecjak, and L. L. Yang, Renormalization-group improved predictions for top-quark pair production at hadron colliders, *J. High Energy Phys.* **09** (2010) 097.
- [72] M. Aliev, H. Lacker, U. Langenfeld, S. Moch, P. Uwer, and M. Wiedermann, HATHOR: HAdronic Top and Heavy quarks crOss section calculatoR, *Comput. Phys. Commun.* **182**, 1034 (2011).
- [73] J. Alwall, C. Duhr, B. Fuks, O. Mattelaer, D. G. Öztürk, and C. H. Shen, Computing decay rates for new physics theories with FEYNRULES and MADGRAPH5_AMCNLO, *Comput. Phys. Commun.* **197**, 312 (2015).
- [74] C. Degrande, C. Duhr, B. Fuks, D. Grellscheid, O. Mattelaer, and T. Reiter, UFO – the universal FEYNRULES output, *Comput. Phys. Commun.* **183**, 1201 (2012).
- [75] A. Alloul, N. D. Christensen, C. Degrande, C. Duhr, and B. Fuks, FEYNRULES 2.0 – A complete toolbox for tree-level phenomenology, *Comput. Phys. Commun.* **185**, 2250 (2014).
- [76] A. Crivellin and L. Mercolli, $B \rightarrow X_d \gamma$ and constraints on new physics, *Phys. Rev. D* **84**, 114005 (2011).
- [77] T. Aaltonen *et al.* (CDF Collaboration), Measurement of the Single Top Quark Production Cross Section and $|V_{tb}|$ in Events with One Charged Lepton, Large Missing Transverse Energy, and Jets at CDF, *Phys. Rev. Lett.* **113**, 261804 (2014).